iScience

CellPress
OPEN ACCESS

Article

# Secretion of WNT7A by UC-MSCs assist in promoting the endometrial epithelial regeneration

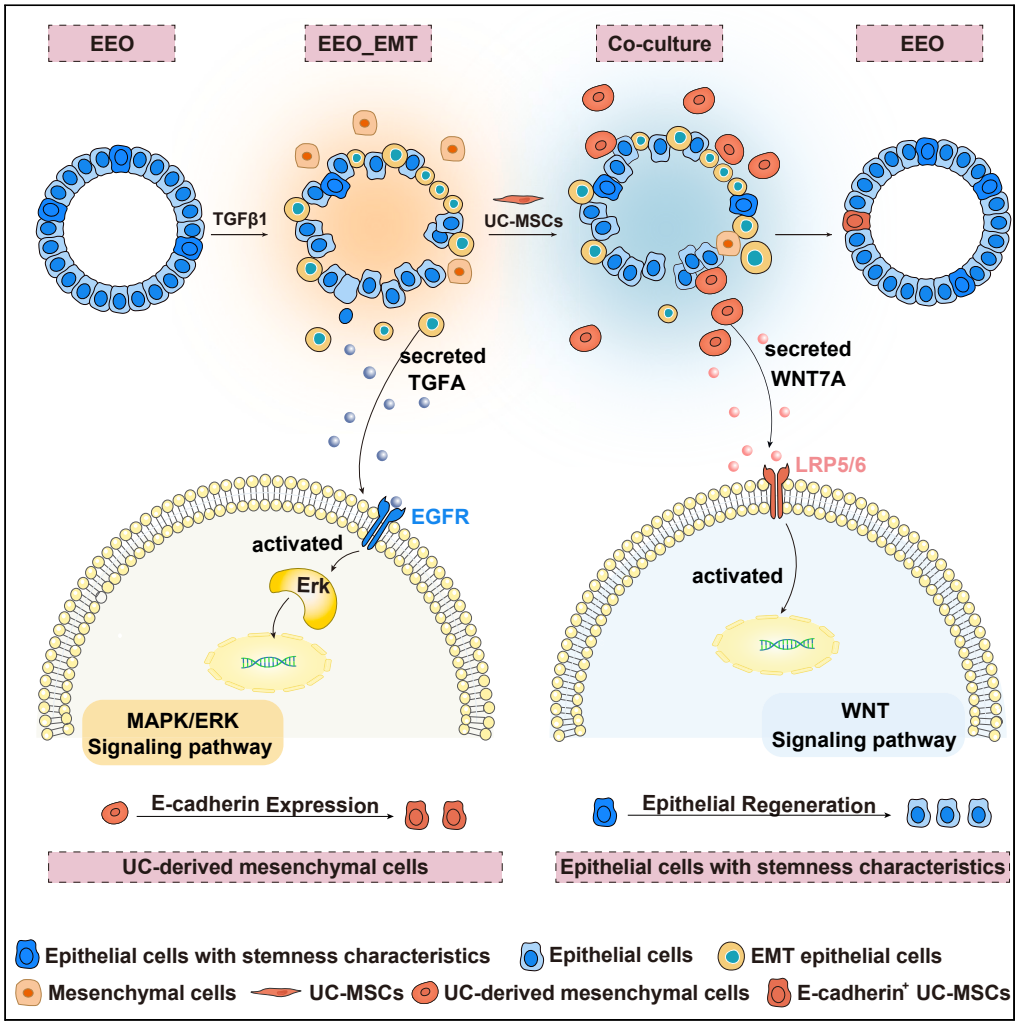


Fangbo Liu, Qin Lin, Shaolei Shen, ..., Yin Long, Juan Wang, Li Liu

longyin@fmmu.edu.cn (Y.L.)
juanwangjuan@aliyun.com (J.W.)
liulisipi@foxmail.com (L.L.)

## Highlights

ECM-adhesion mimic hydrogels effectively replicate endometrial ECM adhesion

UC-MSCs reverse the TGF-β1-induced EMT process

LGR5$^+$ epithelial cells play a pivotal role in organoid formation and growth

Wnt7A secreted by UC-MSCs effectively promotes the proliferation of LGR5$^+$ epithelial cells

Liu et al., iScience 27, 109888
June 21, 2024 
https://doi.org/10.1016/j.isci.2024.109888

iScience

CellPress
OPEN ACCESS

Article

# Secretion of WNT7A by UC-MSCs assist in promoting the endometrial epithelial regeneration

Fangbo Liu,[1,5] Qin Lin,[2,3,5] Shaolei Shen,[1] Zhihong Li,[1] Xiaorui Xie,[1] Quan Cheng,[1] Lan Wang,[1] Yin Long,[4,*] Juan Wang,[1,*] and Li Liu[1,6,*]

## SUMMARY

**Stem cell therapy for intrauterine adhesions (IUAs) has been widely used in clinical treatment. However, intravenous injection lacks sufficient targeting capabilities, while *in situ* injection poses challenges in ensuring the effective survival of stem cells. Furthermore, the mechanism underlying the interaction between stem cells and endometrial cells *in vivo* remains poorly understood, and there is a lack of suitable *in vitro* models for studying these problems. Here, we designed an extracellular matrix (ECM)-adhesion mimic hydrogel for intrauterine administration, which was more effective than direct injection in treating IUAs. Additionally, we analyzed the epithelial-mesenchymal transition (EMT) and confirmed that the activation of endometrial epithelial stem cells is pivotal. Our findings demonstrated that umbilical cord mesenchymal stem cells (UC-MSCs) secrete WNT7A to activate endometrial epithelial stem cells, thereby accelerating regeneration of the endometrial epithelium. Concurrently, under transforming growth factor alpha (TGFA) stimulation secreted by the EMT epithelium, UC-MSCs upregulate E-cadherin while partially implanting into the endometrial epithelium.**

## INTRODUCTION

Intrauterine adhesions (IUAs) are a pathological process characterized by tissue repair failure and excessive fibrosis following endometrial injury, resulting in the replacement of endometrial tissue with fibrotic scars and progressive closure of the uterine cavity.[1,2] The treatment of IUAs aims to facilitate regeneration of the damaged endometrium and restore normal uterine cavity morphology. The standard treatment for IUAs involves hysteroscopic adhesiolysis, followed by estrogen administration to promote endometrial regeneration.[1–3] This approach demonstrates greater efficacy in nonsevere and moderate cases, but finding an effective curative treatment for severe patients remains challenging due to extensive basal layer destruction and poor response to estrogen therapy.[1,4,5] In clinical practice, successful endometrial repair relies on re-epithelialization of the uterine cavity; therefore, postsurgical application of stem cell therapy holds promise as a potential breakthrough strategy. Currently, numerous studies have reported the therapeutic efficacy of stem cells on the endometrial tissue of patients with IUAs. Kilic et al. treated uterine injury mice with adipose mesenchymal stem cells and noted the upregulation of proliferative cells and angiogenic signaling through increased expression levels of VEGF and Ki-67.[6] Clinically, Santamaria et al. administered bone marrow mesenchymal stem cells to 11 patients with IUAs. Most patients exhibited significant improvement, and three of them achieved spontaneous pregnancy.[7–9]

In current stem cell therapy, intravenous injection and *in situ* injection are the most commonly employed methods. However, for IUAs, traditional injection methods are not particularly suitable. Typically, after intravenous injection, a significant number of stem cells become trapped in the lungs before homing to the damaged site. Specifically, in addition to the inherent safety risk of pulmonary embolism, addressing insufficient blood supply to the uterine cavity due to adhesions and vascular necrosis is challenging for patients with IUAs.[10] Furthermore, *in situ* injection has limitations due to the surgical complexity of the procedure, and it is unable to ensure the effective survival of stem cells.[3,5,11,12] Additionally, comprehensive research on changes in the phenotypic characteristics of the endometrial epithelial cell population in patients with IUAs is lacking; similarly, there is limited understanding of the mechanism by which stem cells promote regeneration of the endometrial epithelium.[2,6,7,13–17] Moreover, there is inadequate availability of sufficient *in vitro* models for studying the dynamic interaction between the endometrial epithelial cell population and stem cells.

[1]Shanghai Drugability Biomass Product Evaluation Professional Public Service Platform, Center for Pharmacological Evaluation and Research, China State Institute of Pharmaceutical Industry, No. 285 Gebaini Road, Shanghai 201203, China
[2]The International Peace Maternity and Child Health Hospital, School of Medicine, Shanghai Jiao Tong University, Shanghai 200030, China
[3]Shanghai Key Laboratory of Embryo Original Diseases, Shanghai 200030, China
[4]Department of Traditional Chinese Medicine, Xijing Hospital, Fourth Military Medical University, Xi'an, Shaanxi 710032, China
[5]These authors contributed equally
[6]Lead contact
*Correspondence: longyin@fmmu.edu.cn (Y.L.), juanwangjuan@aliyun.com (J.W.), liulisipi@foxmail.com (L.L.)
https://doi.org/10.1016/j.isci.2024.109888

In this study, we developed a novel hydrogel scaffold for stem cell encapsulation. Additionally, we successfully established an epithelial–mesenchymal transition (EMT) model using endometrial epithelial organoids (EEOs). Subsequently, we confirmed that endometrial epithelial cells differentiate into mesenchymal cells under the influence of TGF-β1. We then analyzed the process of umbilical cord mesenchymal stem cell (UC-MSC)-mediated MET. Furthermore, we elucidated the mechanism by which UC-MSCs promote endometrial epithelial regeneration. Moreover, we confirmed that endometrial epithelial cells with stemness characteristics play a pivotal role in this process and identified the signaling factors involved.

## RESULTS

### UC-MSC-loaded extracellular matrix (ECM)-adhesion mimic hydrogels can be used to effectively treat uterine injury

To develop a scaffold capable of loading UC-MSCs, we utilized the protein types of the endometrial extracellular matrix as a reference to simulate tissue-specific adhesion within the extracellular matrix. First, uterine tissue was obtained from healthy Sprague-Dawley (SD) rats during the estrous interphase and subjected to protein type analysis using liquid chromatography-mass spectrometry (LC-MS). Subsequently, the matrisome proteins in the samples were filtered according to the ECM matrisome database.[18,19] In general, core matrisome proteins remain stable and exhibit minimal variation in response to physiological changes, whereas secreted factors, ECM regulators and ECM-affiliated proteins exhibit significant variability under different physiological conditions.[20–22] We successfully identified 19 core matrisome proteins in our samples. Among them, the expression levels of adhesion proteins, including FN1, LAMB2, COL1A1, and COL1A2, were remarkably prominent (Figures 1A and 1B). We utilized these protein types as a basis to simulate endometrial ECM adhesion. We substituted proteoglycan with 8-arm maleimide-PEG as the basic skeleton structure. Additionally, we incorporated the COL1-derived peptide GFOGER, the LAMB-derived peptide YIGSR and the FN-derived peptide PHSRN to replace COL1A1, COL1A2, LAMB2 and FN1. To further enhance cell adhesion, we supplemented cells with GRGDS adhesion peptide.[23–29] Finally, we used MSC medium as the fundamental solvent to maintain an optimal growth environment for UC-MSCs (Figures 1C–1E).

UC-MSCs were initially generated by SNC Stemcell Biotech for subsequent experiments (Figure S4). UC-MSCs were resuspended in a peptide solution, followed by the addition of 8-arm PEG maleimide to the solution. Gentle shaking at 37°C for 15 min was performed to complete the gel cross-linking process and ensure homogeneous encapsulation of MSCs within the hydrogel. Subsequently, we tested the basic properties of the hydrogel. In comparison to those cultivated in traditional 2D culture, UC-MSCs cultivated within the 3D hydrogel microenvironment exhibited increased proliferation and accelerated adhesion (Figures S1A–S1D). The invasion ability of UC-MSCs in hydrogels was also comparable to that in Matrigel (Figures S1E and S1F).[30–33] Once the efficacy of the hydrogel was confirmed, we administered the hydrogel loaded with UC-MSCs directly into the uterine cavity of a rat model of uterine injury to observe its therapeutic effects (Figure 1F).

To compare the therapeutic effects of the UC-MSC+ hydrogel treatment group (U-CMSC+hydrogel), we also divided the rats into a uterine injury model group (uterine injury), hydrogel control group (hydrogel), a UC-MSC solution direct injection group (UC-MSC), and a blank control group (blank). After treatment, the uteri of the rats in the UC-MSC+hydrogel group recovered significantly compared with those in the uterine injury group, and there was no intrauterine fluid accumulation caused by adhesions; the uteri in the UC-MSC+hydrogel group were similar to those in the blank group. However, the uteri of rats in the hydrogel group and UC-MSC group did not recover, and there were still adhesions present (Figure S2A).

Additionally, the endometrial thickness and number of glands increased in both the UC-MSC+hydrogel group and UC-MSC group, and the observations in the UC-MSC+hydrogel group were similar to those in the blank group. However, the increases in endometrial thickness and the number of glands in the hydrogel group were very slight, and there was no difference from those in the uterine injury group (Figures S2B–S2D; uterine injury vs. hydrogel vs. UC-MSC vs. UC-MSC+hydrogel vs. blank; 1.2 ± 1.6 vs. 1.6 ± 2.3 vs. 9.4 ± 7.2 vs. 16.4 ± 13.2 vs. 18.8 ± 10.8; 71.3 ± 68.1 vs. 124.8 ± 103.6 vs. 135.9 ± 57.1 vs. 440.8 ± 242.8 vs. 545.0 ± 88.5 μm, respectively). Subsequently, we assessed the ratio of collagen deposition and the expression of α-smooth muscle actin (α-SMA), both of which are markers of uterine fibrosis, and observed a significant reduction in uterine fibrosis in the UC-MSC+hydrogel group compared with the uterine injury group, which was similar to what was observed in the blank group. Collagen deposition in hydrogel group and UC-MSC group improved to some extent, but the degree of fibrosis was not different from that in the uterine injury group. (Figures S2E–S2H; uterine injury vs. hydrogel vs. UC-MSC vs. UC-MSC+hydrogel vs. blank; 51.5 ± 30.0% vs. 33.5 ± 23.9% vs. 34.1 ± 11.7% vs. 34.4 ± 16.2% vs. 26.5 ± 11.6%; 131.5 ± 16.1% vs. 129.6 ± 11.6% vs. 129.3 ± 15.3 vs. 109.8 ± 12.0 vs. 106.7 ± 15.5, respectively). Furthermore, compared with that in the uterine injury group, we observed increased expression of the endometrial stromal cell marker vimentin in the UC-MSC+hydrogel group, hydrogel group and UC-MSC group, which were close to the result in the blank group, indicating improved endometrial regeneration in the rats (Figures S2I and S2J; uterine injury vs. hydrogel vs. UC-MSC vs. UC-MSC+hydrogel vs. blank; 76.5 ± 40.0 vs. 114.1 ± 18.4 vs. 110.0 ± 13.9 vs. 123.9 ± 12.4 vs. 128.1 ± 11.6, respectively).[5,34–38]

In summary, we developed an ECM-adhesion mimic hydrogel based on endometrial core matrisome protein types that effectively replicates endometrial ECM adhesion. This hydrogel provides a more suitable *in vitro* environment for UC-MSC growth while offering a safer and more convenient approach for treating uterine injury.

### UC-MSCs promote endometrial epithelial cell proliferation and rescue the TGF-β1-induced EMT process

After successful treatment with hydrogel-loaded UC-MSCs, our objective was to clarify the underlying mechanism of UC-MSCs in IUA therapy. Initially, uterine specimens were cultured into endometrial epithelial organoids (EEOs) (Figures S3A–S3C; Table S1).[39–42] Subsequently, the EEO cells were digested into single cells and cocultured with varying ratios of UC-MSCs in Matrigel (0:1, 0.5:1, 1:1, and

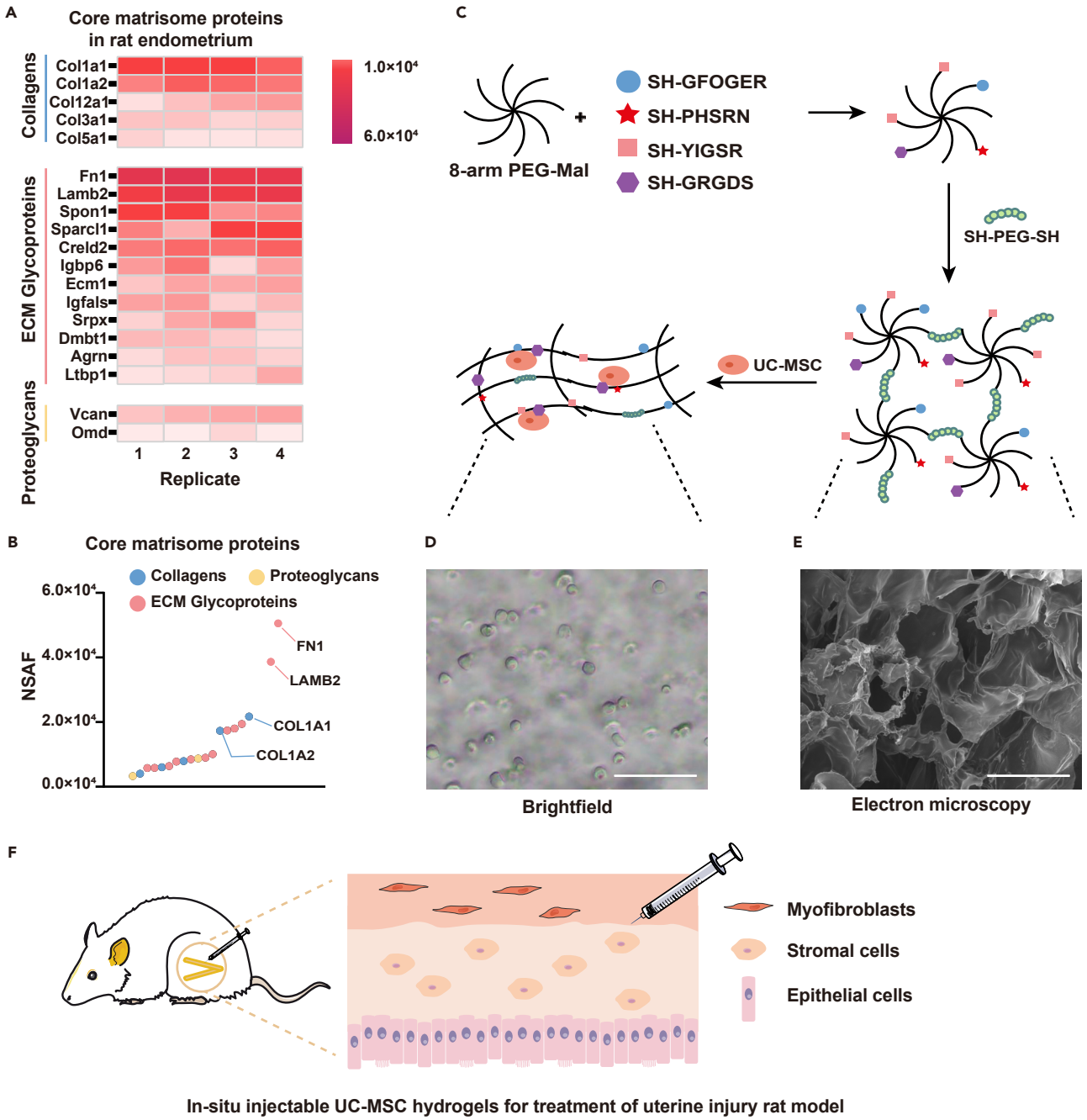


**Figure 1. Development of ECM-adhesion mimic hydrogels and treatment for intrauterine adhesions**

(A) Heatmap of the normalized spectral abundance factor (NSAF) for matrisome proteins in rat uterine tissues ($n$ = 4).

(B) Proportion of matrisome proteins in rat uterine tissues.

(C) Schematic representation of hydrogel synthesis and UC-MSC encapsulation.

(D) Brightfield image of hydrogel-loaded UC-MSCs (scale bar: 100 μm).

(E) Electron microscopy image of the hydrogel (scale bar: 200 μm).

(F) Schematic representation of the treatment for IUA rats.

2:1 UC-MSCs:EEO cells). Following a 10-day culture period, increases in both the number and diameter of EEOs were observed as the ratio of UC-MSCs increased, indicating that UC-MSCs effectively promoted the proliferation of endometrial epithelial cells and the regeneration of endometrial epithelium (Figure 2A).

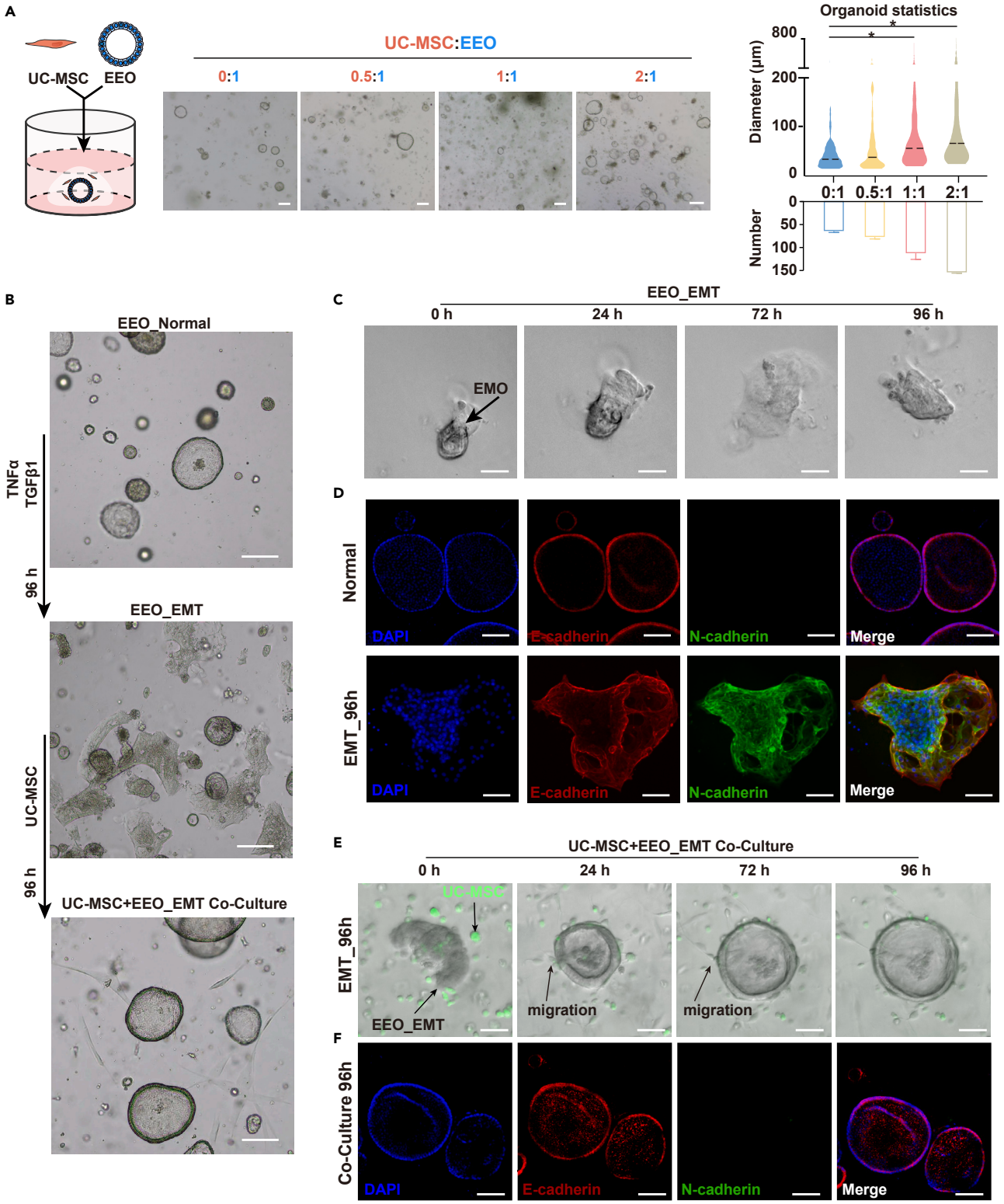


**Figure 2. UC-MSC promote endometrial epithelial cell proliferation and reverse the EMT process**

(A) Organoid formation efficiency of EEO cells cocultured with UC-MSCs (scale bar: 100 μm, $n = 3$, $^*p < 0.05$).

(B) Brightfield images of normal EEO, EMT-induced EEO, and UC-MSCs+EMT-induced EEO (scale bar: 100 μm).

**Figure 2. *Continued***

(C) Time-lapse recording of the EMT process (scale bar: 100 μm).

(E) Time-lapse recording of the MET process after coculture of UC-MSCs and EMT-induced EEO (scale bar: 100 μm).

(D) and (F) Immunofluorescence staining of E-cadherin and vimentin (scale bar: 100 μm).

It has been reported that EMT plays a crucial role in the pathogenesis of IUAs, where an accumulation of mesenchymal cells leads to the formation of adhesions and subsequent uterine closure.[39,43–46] In our *in vitro* experiment, we aimed to induce EMT in endometrial epithelial organoids.[40,41] Following EEO passage, two cytokines, TNFα and TGF-β1, were added to the culture medium on the first day (Figure 2B). Over a 96-h culture period, gradual shedding of cells from EEOs was observed along with a change in their morphology from a transparent spherical shape toward an opaque irregular shape that tended to adhere to the walls of the plate wells. In severe cases, complete maintenance of the EEO structure was compromised, as the shed cells migrated from the Matrigel toward the bottom of the well plate and acquired a spindle-like appearance (Figures 2B and 2C; Figure S3D). Immunofluorescence staining revealed the expression of N-cadherin, a specific marker of mesenchymal cells, in these irregularly shaped organoids at this stage, indicating the occurrence of the EMT process within EEOs (Figure 2D).

Subsequently, EMT-induced EEOs and UC-MSCs were coinoculated in Matrigel (1:1, UC-MSCs: EMT-induced EEO cells), followed by a 96-h coculture period. Remarkably, we observed a complete restoration of the EEO morphology, with a reversion to its original transparent spherical shape (Figures 2B and 2E). Immunofluorescence staining revealed the expression of the epithelial marker E-cadherin within the organoids but the absence of the expression of the mesenchymal marker N-cadherin (Figure 2F), indicating that following interaction with UC-MSCs, the previously induced EMT underwent MET and successfully regenerated into a normal EEO.

Finally, we excluded epithelial cells with stemness characteristics from the EEO as much as possible to further confirm the occurrence of EMT and MET. LGR5 has been suggested to be a potential marker for the endometrial epithelium, but it has not yet been established as a specific marker for endometrial epithelial stem cells. However, considering its role as a general stem cell marker, we employed LGR5 as an indicator of "stemness characteristics" in our subsequent investigations.[42,47–50] We sorted LGR5$^{-}$ cells, induced EMT, and then cocultured them with UC-MSCs (1:1, UC-MSCs:LGR5$^{-}$ cells, Figures S3E and S3F). The immunofluorescence staining results were consistent with those shown in Figures 2D and 2F. LGR5$^{-}$ cells were induced to express N-cadherin by the EMT process, and after coculture with UC-MSCs, N-cadherin was no longer expressed.

## Single-cell landscape analysis of the trajectory of EEOs and UC-MSCs

Subsequently, we aimed to elucidate the interaction dynamics between EEOs and UC-MSCs during EMT at single-cell resolution. Initially, the samples were categorized as follows: S1, normal EEOs; S2, EMT-induced EEOs for 96 h; S3, EMT-induced EEOs for 96 h cocultured with UC-MSCs for 12 h (1:1, UC-MSCs: EMT-induced EEO cells); and S4, EMT-induced EEOs for 96 h cocultured with UC-MSCs for 96 h (1:1, UC-MSCs: EMT-induced EEO cells).

We employed the 10× Genomics platform for scRNA-seq, generating a landscape of 34,195 cells from the aforementioned four samples. Then, the filtered cells were grouped into 13 clusters and visualized using Uniform Manifold Approximation and Projection (UMAP) (Figure 3A). Furthermore, cell types were identified based on the expression profiles of known markers, and these cell clusters could be divided into seven categories: luminal epithelial cells (luminal epi), glandular epithelial cells (glandular epi), EMT epithelial cells (EMT epi), proliferating EMT epithelial cells (proliferating epi), mesenchymal cells (Mes), UC-MSCs, and UC-derived mesenchymal cells (UC-derived mes).[51,52–60] Notably, the UC-MSCs utilized in this study were derived from male donors and expressed Y chromosome-specific proteins and the mesenchymal marker CDH2 (Figures 3C; Figure 4A).

Subsequently, we observed that luminal epi and glandular epi constituted the dominant cell types in sample S1. In sample S2, which underwent EMT induction for 96 h, EMT epi and Mes were identified as the primary cell populations. After coculturing with UC-MSCs for 12 h, sample S3 exhibited decreases in the proportions of EMT epi and Mes. Additionally, the proportion of Luminal epi, along with increased in the presence of UC-MSCs and UC-derived mes. Finally, in sample S4, which was cocultured with UC-MSCs for 96 h, luminal epi and glandular epi re-emerged as the predominant cell types, gradually recovering to the levels observed in normal EEO samples (Figure 3B).

Furthermore, we performed a pseudotime trajectory analysis on the sequencing data. The trajectory analysis inferred that during the process of EMT, Mes may be derived from EMT epi. Additionally, after coculture with UC-MSCs, EEOs may have undergone mesenchymal-epithelial transition (MET), enabling Mes to redifferentiate into EMT epi (Figure 3D).

The body secretes a substantial quantity of TGF-β1 in response to factors such as injury and inflammation.[1,22,61,62] Based on the immunostaining, sequencing and pseudotime analysis results (Figures 2 and 3; S3), we infer that the endometrial epithelium initiates the process of EMT under the action of TGF-β1. Initially, both luminal epi and glandular epi gradually exhibit an EMT phenotype, accompanied by high expression levels of EMT-related proteins, including LAMA3, LAMB3, and MACC1. Subsequently, these EMT epi differentiate into Mes. Mes specifically expresses N-cadherin while abundantly occupying the uterine cavity to form adhesions.[1,38,63] One of the mechanisms by which UC-MSCs treat IUAs lies in their ability to reverse the EMT process. The results of immunostaining, sequencing, and pseudotime analysis indicated that the following changes may have occurred after UC-MSCs were added to the coculture system: UC-MSCs were initially influenced by the microenvironment dominated by EMT epi and Mes, gradually acquiring a mesenchymal phenotype. UC-derived mes exhibited high expression levels of EMT-related proteins, such as LAMA3, LAMB3, and MACC1, while not expressing Y chromosome-specific protein USP9Y (Figure 4A). Next, some UC-derived mes slightly upregulated E-cadherin. Meanwhile, under the paracrine influence of UC-derived mes, Mes also redifferentiated into EMT epi, ultimately reverting from the EMT phenotype back to luminal epi and glandular epi (Figure 4B).

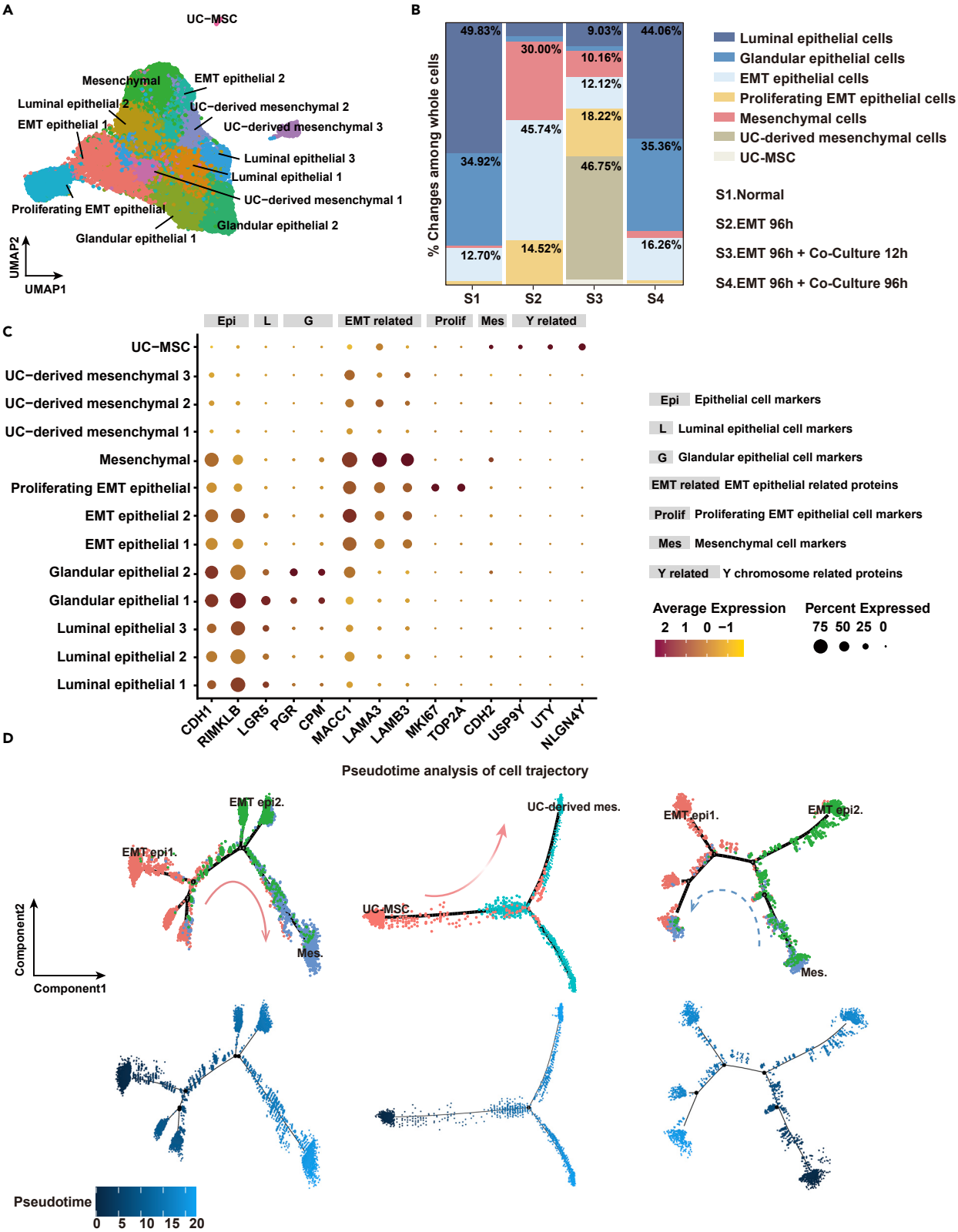
A
UC−MSC
Mesenchymal
EMT epithelial 2
Luminal epithelial 2
UC−derived mesenchymal 2
EMT epithelial 1
UC−derived mesenchymal 3
Luminal epithelial 3
Luminal epithelial 1
UC−derived mesenchymal 1
Proliferating EMT epithelial
Glandular epithelial 2
Glandular epithelial 1
UMAP2
UMAP1
B
% Changes among whole cells
49.83%
34.92%
12.70%
30.00%
45.74%
14.52%
9.03%
10.16%
12.12%
18.22%
46.75%
44.06%
35.36%
16.26%
S1
S2
S3
S4
Luminal epithelial cells
Glandular epithelial cells
EMT epithelial cells
Proliferating EMT epithelial cells
Mesenchymal cells
UC-derived mesenchymal cells
UC-MSC
S1.Normal
S2.EMT 96h
S3.EMT 96h + Co-Culture 12h
S4.EMT 96h + Co-Culture 96h
C
Epi
L
G
EMT related
Prolif
Mes
Y related
UC−MSC
UC−derived mesenchymal 3
UC−derived mesenchymal 2
UC−derived mesenchymal 1
Mesenchymal
Proliferating EMT epithelial
EMT epithelial 2
EMT epithelial 1
Glandular epithelial 2
Glandular epithelial 1
Luminal epithelial 3
Luminal epithelial 2
Luminal epithelial 1
CDH1
RIMKLB
LGR5
PGR
CPM
MACC1
LAMA3
LAMB3
MKI67
TOP2A
CDH2
USP9Y
UTY
NLGN4Y
Epi Epithelial cell markers
L Luminal epithelial cell markers
G Glandular epithelial cell markers
EMT related EMT epithelial related proteins
Prolif Proliferating EMT epithelial cell markers
Mes Mesenchymal cell markers
Y related Y chromosome related proteins
Average Expression
2 1 0 −1
Percent Expressed
75 50 25 0
D
Pseudotime analysis of cell trajectory
EMT epi2.
EMT epi1.
Mes.
UC-derived mes.
UC-MSC.
EMT epi1.
EMT epi2.
Mes.
Component2
Component1
Pseudotime
0 5 10 15 20

**Figure 3. Single-cell landscapes revealed the trajectory of EEOs and UC-MSCs**

(A) UMAP plot of scRNA-seq data from a total of 4 individual samples, including EEO and UC-MSC samples.

(B) Changes in total cell proportions across 4 samples.

(C) Expression of marker genes of each cell type in the EEO and UC-MSC samples.

(D) The cell trajectory presented by pseudotime analysis.

## Epithelial cells with stemness characteristics are crucial to the epithelial regeneration process

Our aim was to further elucidate the pivotal factors facilitating the growth of endometrial epithelial organoids. First, epithelial cells were filtered from single-cell analysis sample S4 (cocultured for 96 h) and classified into PROM1$^{+}$ and PROM1$^{-}$ populations. PROM1, a protein expressed on endometrial epithelial progenitor cells, was also found to be expressed in all differentiated epithelial cells derived from these progenitors but was not expressed in UC-MSCs.[54,64] Thus, it was utilized to distinguish differentiated epithelial cells from exogenous UC-MSCs. In sample S4, out of a total of 8,061 epithelial cells, 195 PROM1$^{-}$ cells accounted for 2.4% of the cells (Figure 5A). This result was further validated by flow cytometry (Figure 5B; Figures S5A–S5C).

Next, we labeled UC-MSCs with CFSE and then uniformly incubated them with an anti-E-cadherin antibody after 96 h of coculture with EMT-induced EEOs (1:1, UC-MSCs: EMT-induced EEO cells). The percentage of CFSE$^{+}$ and E-cadherin$^{+}$ cells was 1.8 $\pm$ 0.17% (Figure 5C; Figure S5D). We continued to verify the changes in UC-MSCs by immunofluorescence and found that they expressed only E-cadherin and did not express other epithelial markers, such as keratin. Additionally, we cocultured normal EEOs with UC-MSCs and found that UC-MSCs did not express any epithelial markers (Figures 5D and 5E). Collectively, these findings suggest that in the EMT microenvironment, only a small number of UC-MSCs are implanted in EEOs, and their contribution to epithelial formation is minimal compared to that of endogenous endometrial epithelial cells.

Therefore, we hypothesized that the activation of endometrial epithelial cells with stemness characteristics is crucial for promoting EEO formation (or endometrial epithelial regeneration). We subsequently sorted LGR5$^{+}$ and LGR5$^{-}$ endometrial epithelial cells from normal EEOs and subjected them to organoid culture (Figure 5F). Remarkably, under identical culture conditions, LGR5$^{+}$ endometrial epithelial cells exhibited a significantly greater number and diameter of organoids than normal unsorted cells. In contrast, LGR5$^{-}$ endometrial epithelial cells with smaller diameters showed limited organoid formation ability and could not even be passaged. Furthermore, when cocultured with UC-MSCs (UC-MSCs:EEO cells, 1:1), the LGR5$^{-}$endometrial epithelial cell population did not change this situation (Figures 5G and 5H), indicating that endogenous stem cells play a pivotal role in organoid formation and growth.

Based on the above results, we further investigated the potential of UC-MSCs to promote endometrial epithelial regeneration. We extended the duration of EMT induction from 96 h to 120 and 144 h, followed by coculture with UC-MSCs. Notably, no endometrial epithelial regeneration was observed in EMT-induced EEOs at 120 and 144 h (Figure 6A).

Subsequently, we assessed the proportion of LGR5$^{+}$ cells in EEOs subjected to different durations of EMT induction. The percentage of these cells in the normal organoids was 5.10 $\pm$ 0.21%, while it decreased to 2.24 $\pm$ 0.17% after EMT induction for 96 h, further decreased to 1.05 $\pm$ 0.43% after EMT induction for 120 h, and reached a minimum of only 0.37 $\pm$ 0.21% following EMT induction for 144 h (Figure 6B; Figures S5E–S5H). Hence, our findings confirm that exogenous UC-MSCs are unable to promote endometrial epithelial regeneration when there is an insufficient population of endogenous cells with stemness. Therefore, as the duration of EMT increases, the proportion of endogenous cells with stemness within EEOs significantly decreases. Consequently, exogenous UC-MSCs are unable to promote endometrial epithelial regeneration.

## Wnt7A and TGFA play roles in the interaction between EEOs and UC-MSCs

Subsequently, we endeavored to further investigate the specific factors that facilitate the interaction between endogenous epithelial cells and exogenous UC-MSCs. We performed cell communication and Kyoto Encyclopedia of Genes and Genomes (KEGG) analyses to elucidate the signaling molecules and pathways involved in the interaction between EEOs and UC-derived mesenchymal cells. Initially, KEGG analysis revealed significant activation of the MAPK signaling pathway in the 96-h EMT sample, while the 96-h coculture sample exhibited pronounced activation of the Wnt signaling pathway (Figure 6C). Furthermore, our investigation into the cell communication of UC-derived mesenchymal cells revealed the high expression of the Wnt7A-LDLR pair. ELISA detection of the supernatant also confirmed an increasing trend in the Wnt7A concentration within cocultured samples over time (Figures 7A–7C). These findings imply that the secretion of Wnt7A by UC-derived mesenchymal cells stimulates endometrial epithelial proliferation.

Therefore, we sorted EEO_EMT cells and retained the LGR5$^{+}$ cell population. We cultured LGR5$^{+}$ cells in EMT medium, and in the absence of Wnt7A, the cell population did not form organoids. After the addition of Wnt7A (112 ng/mL; the concentration was referred to in Figure 7C: 96 h concentrations of Wnt7A), the cell population successfully formed organoids (Figures 7D and 7E). We also detected the proliferation of LGR5$^{+}$ cells in Matrigel with different concentrations of Wnt7A. The data showed that the LGR5$^{+}$ cells in the 93 and 112 ng/mL Wnt7A groups (Figure 7C: 12 h and 96 h concentrations of Wnt7A, respectively) showed proliferation, while the cells did not show significant proliferation without the addition of Wnt7A (Figure 7F). Combined with the aforementioned results, it is clear that Wnt7A indeed promotes epithelial cell proliferation.

Subsequently, we observed significant upregulation of the Transforming growth factor alpha-Epidermal growth factor receptor (TGFA-EGFR ) pair in the cell communication of EMT epithelial cells. ELISA analysis of the supernatant revealed a trend characterized by an initial increase followed by a subsequent decrease in the TGFA concentration, with its peak at 12 h and minimal levels at 96 h (Figures 7A and 7C). Furthermore, western blot analysis demonstrated that p-Erk expression varied over time, with the highest level observed at 12 h and reduced expression at 96 h (Figures 7G and 7H).

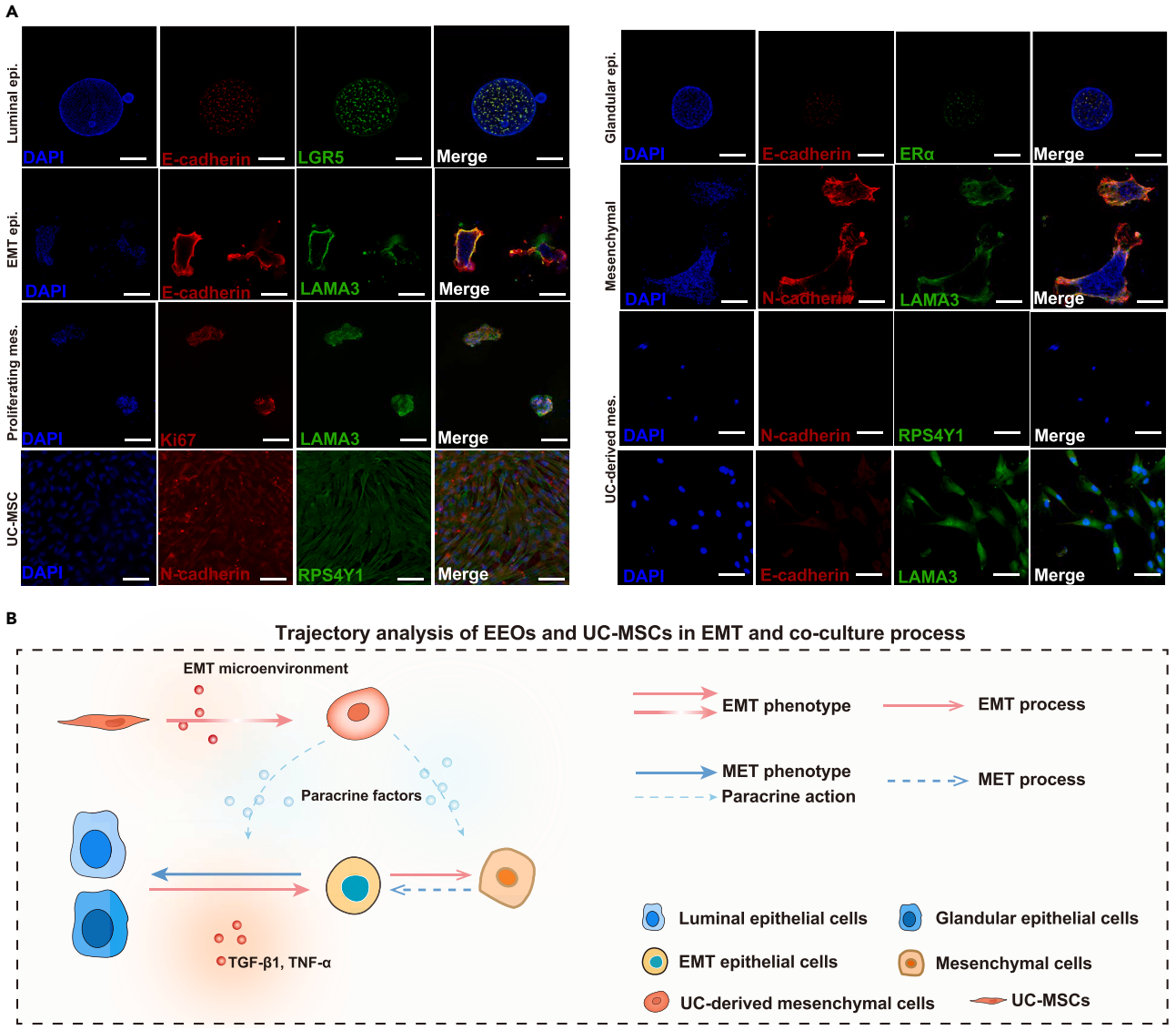


**Figure 4. Immunofluorescence staining to validate markers of cell populations among EEOs and UC-MSCs**

(A) Immunofluorescence images of markers for luminal epithelial cells (luminal epi), glandular epithelial cells (glandular epi), EMT epithelial cells (EMT epi), proliferating EMT epithelial cells (proliferating epi), mesenchymal cells (Mes), UC-MSCs, and UC-derived mesenchymal cells (UC-derived mes) (scale bar: 100 μm).
(B) Schematic representation of the trajectory analysis of the EMT and coculture processes.

These results imply that in the EMT microenvironment, TGFA activates the downstream MAPK/ERK signaling pathway of EGFR, which ultimately upregulates the expression of E-cadherin in UC-MSCs.[65–69] To verify this process, we cultured UC-MSCs alone in Matrigel (EMT medium) and added TGFA to the EMT medium (52 and 26 ng/mL; the concentration was referred to Figure 7C: 12 h and 96 h concentrations of TGFA, respectively). After 96 h of culture, we found that UC-MSCs in the 52 ng/mL group expressed E-cadherin, while UC-MSCs in the 26 ng/mL group did not (Figures 7I and 7J). These results indicate that high concentrations of TGFA upregulate E-cadherin expression in UC-MSCs, but when the concentration of TGFA is too low, UC-MSCs do not express E-cadherin. These results also explain why the proportion of E-cadherin$^{+}$ UC-MSCs was very small because high concentrations of TGFA did not persist for a long time. Moreover, we found that UCMSCs did not upregulate the expression of PanCK or ERα, indicating that TGFA only upregulated the expression of E-cadherin and did not induce epithelial differentiation of UC-MSCs (Figures S3G and S3H).

## DISCUSSION

Currently, the occurrence of pulmonary embolism resulting from intravenous injection of stem cells is not uncommon; Jung et al. reported a clinical case involving pulmonary embolism following intravenous administration of adipose-derived stem cells.[10] Furthermore, due to severe

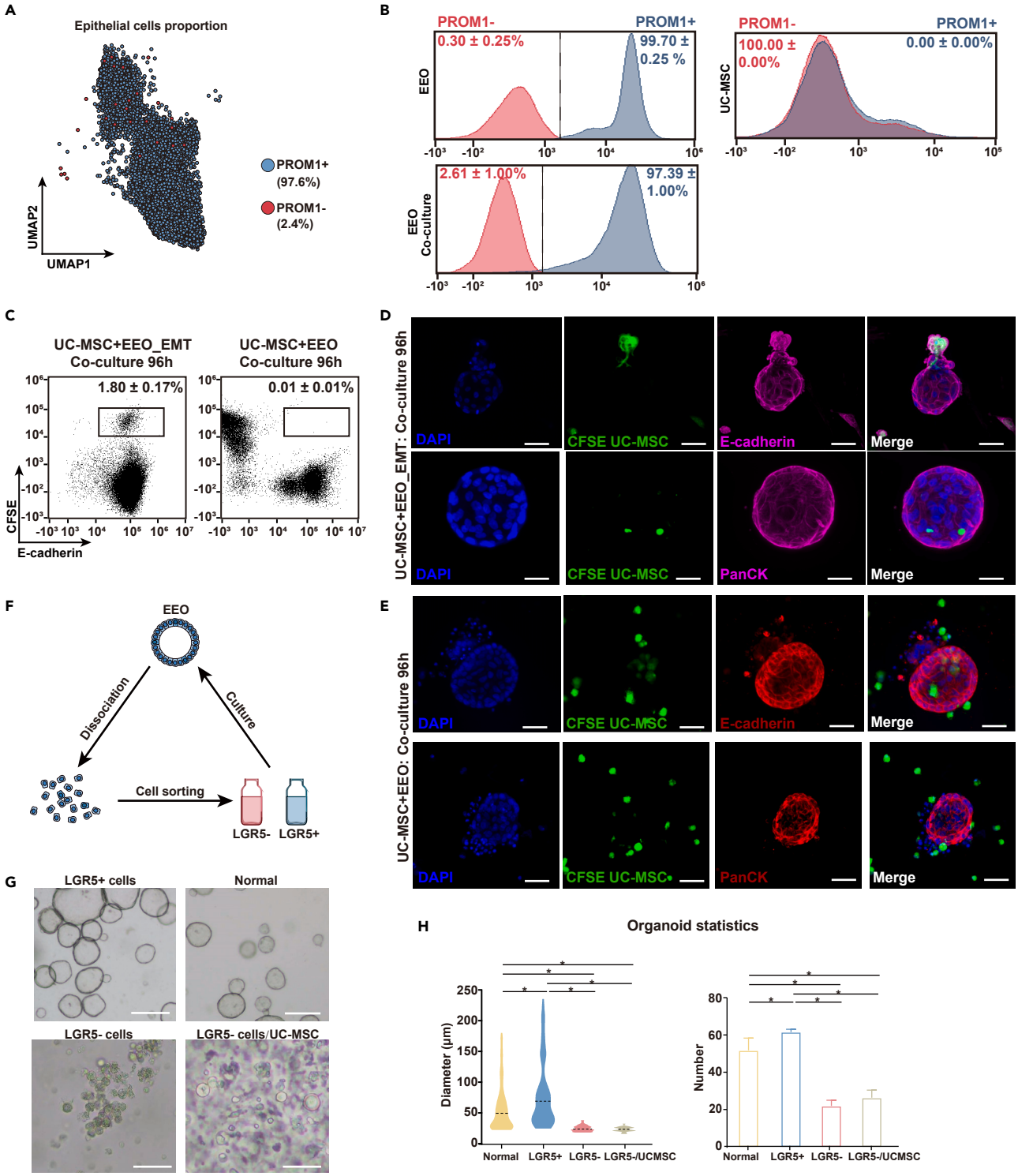


**Figure 5. Epithelial cells with stemness characteristics are crucial to the epithelial regeneration process**

(A) Expression of PROM1 in epithelial cells after coculture with UC-MSCs.

(B) Histogram plot showing the PROM1-and PROM1+ populations in EEO cells and UC-MSCs ($n$ = 3; replicates are shown in Figures S5A–S5C).

(C) Dot plot showing CFSE+ and E-cadherin+ populations in EEO_EMT and normal EEO cells cocultured with UC-MSCs ($n$ = 3; replicates are shown in Figure S5D).

**Figure 5. *Continued***

(D) Immunofluorescence staining to validate the presence of the E-cadherin and PanCK proteins in the cell populations among the EEO_EMT and UC-MSCs (scale bar: 100 μm).

(E) Immunofluorescence staining to validate the presence of the E-cadherin and PanCK proteins in the cell populations among the normal EEO and UC-MSC (scale bar: 100 μm).

(F) Schematic representation of cell sorting of $LGR5^+$ and $LGR5^-$ cell populations.

(G) Different behaviors were observed between the $LGR5^+$ and $LGR5^-$ cell populations. Bright field images of $LGR5^+$ cells, $LGR5^-$ cells and $LGR5^-$ cells+UC-MSCs are shown (scale bar: 100 μm).

(H) Organoid formation efficiency of LGR5+ cells, $LGR5^-$ cells and $LGR5^-$ cells+UC-MSCs ($n = 3$, $^*p < 0.05$).

adhesion and extensive capillary necrosis, it remains uncertain whether stem cells can accurately target the injury area.[34] Therefore, we developed a cell scaffold suitable for *in situ* injection while minimizing the risks associated with pulmonary embolism and inadequate targeting. Our hydrogel successfully achieved our anticipated objectives, rendering it a more convenient and secure approach for treating uterine injury in rats. Moreover, the endometrial morphology indicated significant recovery of the uterine injury in the rat model treated with hydrogel-loaded UC-MSCs, accompanied by a notable reduction in fibrosis and successful restoration of the regenerative capacity within the endometrium.[1,5,35]

Subsequently, we investigated the interaction trajectory between endogenous cells and UC-MSCs. Initially, we observed unequivocal evidence for the ability of stem cells to promote endometrial epithelium proliferation. However, our progress has been hindered by a lack of *in vitro* models specifically designed for studying IUAs. Consequently, we constructed an organoid model based on the pathogenesis of IUAs and specifically focused on EMT, a pivotal contributor to adhesion formation.[2,62] Our EMT model was designed to simulate this process. During the induction process, the EEOs were first incubated with Tryple and trypsin at 37°C for 5 min. Subsequently, without quenching the incubation, centrifugation was performed (300 × g, 5 min) directly to maximize the disruption of intercellular connections. In addition, the medium was supplemented with TNF-α and TGF-β1; the former is a crucial cytokine in inflammatory environments, and the latter serves as a key inducer of EMT.[70] Then, the expression of the mesenchymal cell marker N-cadherin was validated when noticeable morphological changes occurred (such as gradual cell shedding or transformation from spherical to irregular structures). Our established protocol for constructing an EMT model of EEOs not only facilitates research on IUAs but also offers valuable insights into developing fibrosis models in other tissues.

We also considered the influence of tissue-resident stem cells when constructing the EMT model. Bhartiya, D et al. reported the presence of very small embryonic-like stem cells (VSELs), a type of pluripotent stem cell that can differentiate into epithelial and mesenchymal cells, in the endometrium.[71,72] However, because VSELs can be enriched only upon centrifugation at 1000 × g, we excluded the possibility of the presence of VSELs in our cultured EEO. Second, the endometrial epithelium also contains epithelial resident stem cells. Therefore, we purified $LGR5^-$ cells to eliminate the influence of resident epithelial stem cells as much as possible. Finally, $LGR5^-$ cells also exhibited EMT and MET transformation.

Next, we observed the gradual movement of UC-MSCs around the EMT organoids. We found that the proportion of UC-MSCs implanted into the endometrial epithelium was minimal, raising an additional question: does this imply that UC-MSCs primarily serve as an adjunctive factor rather than a pivotal factor? We next isolated $LGR5^+$ and $LGR5^-$ cells from normal endometrial organoids. We then added UC-MSCs to the culture system of $LGR5^-$ cells; however, no organoid formation was observed. These findings provide preliminary evidence supporting the pivotal role of endogenous epithelial cells with stemness characteristics in endometrial epithelial regeneration.

In addition to epithelial cells, stromal, immune, and endothelial cells are also found in the uteri of patients with IUA. Because our study aimed to focus mainly on the interaction between UC-MSCs and endometrial epithelial cells, we selected EEOs as the experimental model. There have been single-cell sequencing studies on the uteri of patients with IUA. Santamaria, X et al. decoded the endometrium cell populations, differential gene expression, and cell-to-cell communication of IUA tissue as a whole.[59] In contrast, our study focused on the dynamic changes between the endometrial epithelium and UC-MSCs. In addition, Santamaria, X et al. reported that there was no interaction between WNT7AFZD6 and LRP6 in the SOX9 epithelial cell type of patients with IUA, which may slow luminal cell differentiation. This result complements our research findings, indirectly demonstrating the role of UC-MSCs in the secretion of Wnt7A to assist in promoting endometrial epithelial regeneration.

## Limitations of the study

This study focused primarily on the dynamic changes in endometrial epithelial cells in the context of IUA. In addition to the process of EMT, the proliferation of mesenchymal cells and the activation of fibroblasts are also significant factors contributing to adhesion formation. Furthermore, we propose that the paracrine effects of the interaction of MSCs with the EMT epithelium are not solely dependent on a single pathway. In future studies, our next challenge will be to comprehensively elucidate the interplay between the different factors involved and their mechanisms.

## STAR★METHODS

Detailed methods are provided in the online version of this paper and include the following:

- KEY RESOURCES TABLE
- RESOURCE AVAILABILITY

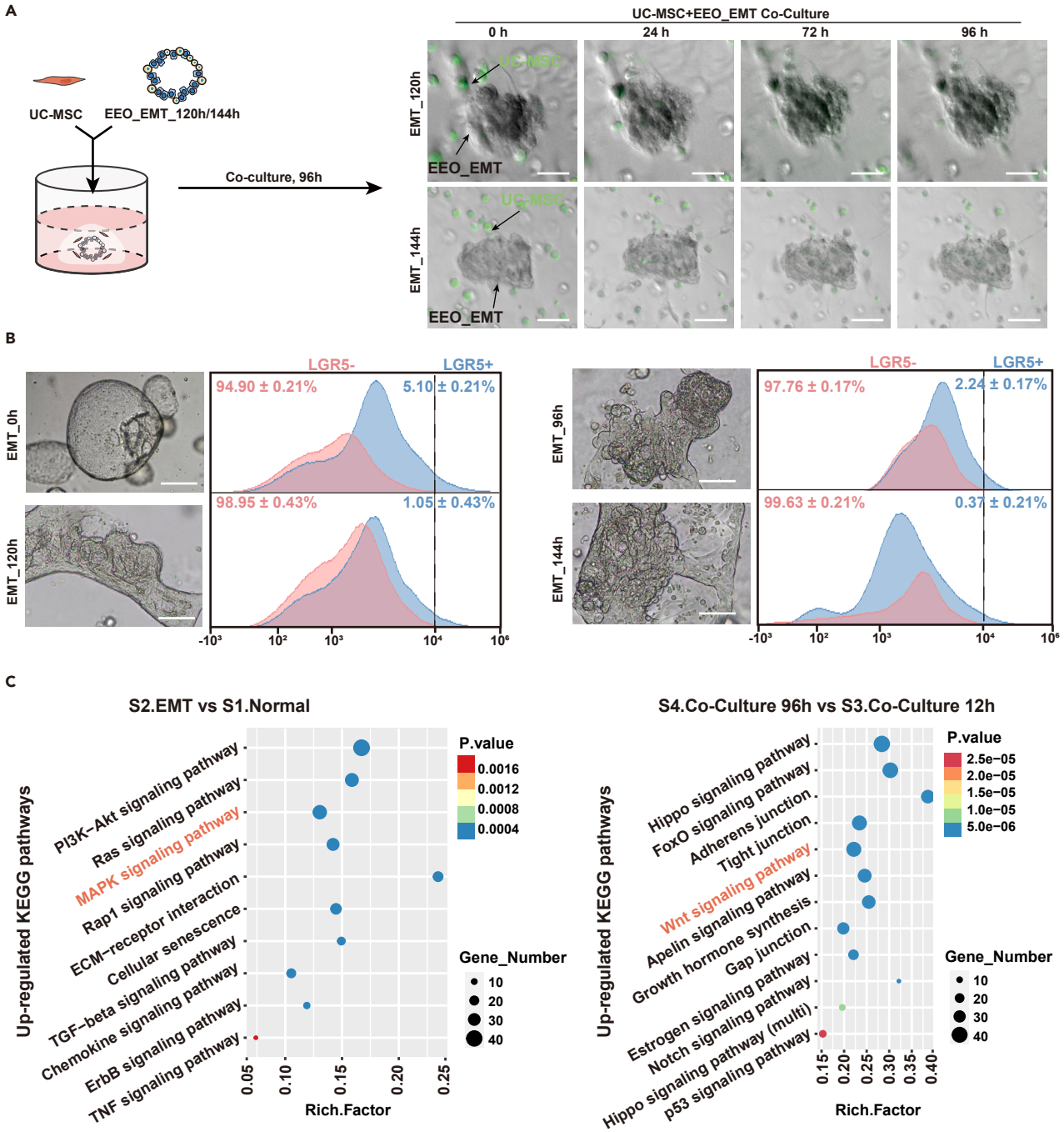


**Figure 6. Ratios of epithelial cells with stemness characteristics and up-regulated pathways after EMT induction and co-culture**

(A) Time-lapse recording of EMT 120 and 144 h groups (scale bar: 50 μm).

(B) Bright field images of normal EEO and EMT induced EEO (scale bar: 100 μm). Histogram plot showing LGR5$^{-}$ and LGR5+ populations in EEO cells ($n$ = 3; replicates are shown in Figures S5E–S5H).

(C) KEGG analysis shows upregulated pathways in EMT 96 h and coculture 96 h samples.

- ○ Lead contact
- ○ Materials availability
- ○ Data and code availability

● EXPERIMENTAL MODEL AND STUDY PARTICIPANT DETAILS

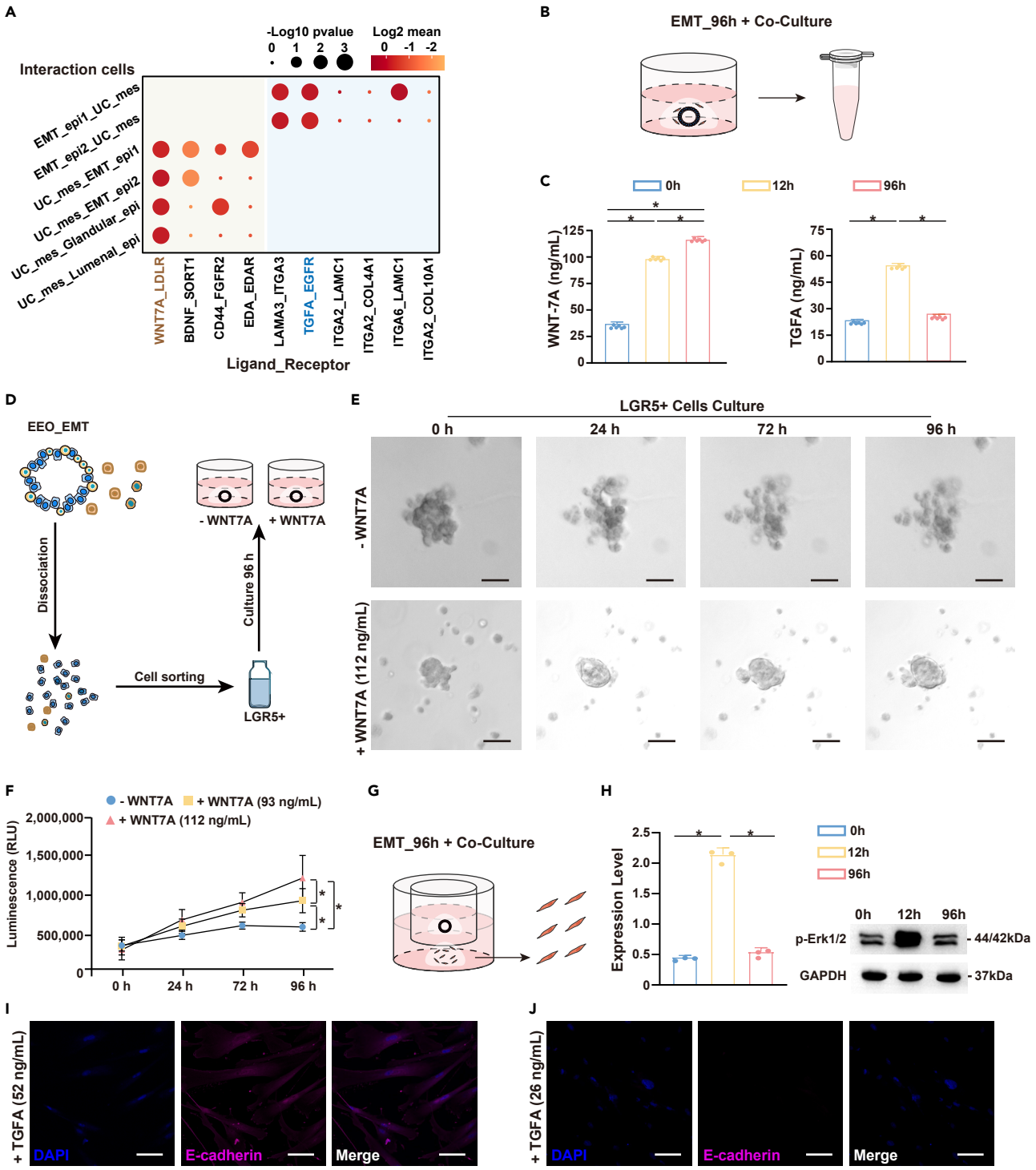


**Figure 7. Wnt7A and TGFA are signaling molecules in the interaction between EEOs and UC-MSCs**

(A) Cell communication connections between EMT epithelial cells and UC-derived mesenchymal cells.

(B) Schematic representation of Wnt7A and TGFA detection.

(C) Concentration statistics of Wnt7A and TGFA ($n = 6$, $^*p < 0.05$).

(D) Schematic representation of cell sorting in LGR5+ cell populations.

(E) Time-lapse recording of the group supplemented with WNT7A (112 ng/mL) and the group without WNT7A (scale bar: 50 μm).

(F) Cell Viability of WNT7A-supplemented groups (112 ng/mL and 93 ng/mL), and group without WNT7A ($n = 3$, $^*p < 0.05$).

**Figure 7. *Continued***

(G) Schematic representation of p-Erk1/2 detection and immunofluorescence validation of E-cadherin.

(H) Detection of p-Erk1/2 expression level ($n = 3$, $^*p < 0.05$).

(I) and (J) Immunofluorescent staining to detect E-cadherin of UC-MSCs in groups supplemented with TGFA (52 ng/mL and 26 ng/mL; scale bar: 100 μm).



## SUPPLEMENTAL INFORMATION

Supplemental information can be found online at https://doi.org/10.1016/j.isci.2024.109888.


## ACKNOWLEDGMENTS

This work was supported by China State Institute of Pharmaceutical Industry, "Graduate Innovation Fund" (21DZ2290100).


## AUTHOR CONTRIBUTIONS

L.-L. and F.-L. conceived the study and designed the research. L.-L., J.-W., and Y.-L. jointly supervised the study. F.-L. contributed to validation experiments. L.-W., X.-X., and Q.-C. assisted with validation experiments. Q.-L. contributed to sample collection and pathology review. S.-S. performed bioinformatics analysis with the assistance of F.-L. Z.-L. performed protemic analysis with the assistance of F.-L. L.-L. and F.-L. supervised data analysis, data integration, and interpretation. L.-L., F.-L., and Q.-L. wrote the manuscript. L.-L., J.-W., and Y.-L. revised the manuscript. All authors contributing to the review and editing of the manuscript.

## DECLARATION OF INTERESTS

The authors declare no competing interests.


Received: January 9, 2024
Revised: March 19, 2024
Accepted: April 30, 2024
Published: May 3, 2024


## REFERENCES


1. Deans, R., and Abbott, J. (2010). Review of Intrauterine Adhesions. J. Minim. Invasive Gynecol. *17*, 555–569. https://doi.org/10.1016/j.jmig.2010.04.016.
2. Benor, A., Gay, S., and DeCherney, A. (2020). An update on stem cell therapy for Asherman syndrome. J. Assist. Reprod. Genet. *37*, 1511–1529. https://doi.org/10.1007/s10815-020-01801-x.
3. Azizi, R., Aghebati-Maleki, L., Nouri, M., Marofi, F., Negargar, S., and Yousefi, M. (2018). Stem cell therapy in Asherman syndrome and thin endometrium: Stem cell-based therapy. Biomed. Pharmacother. *102*, 333–343. https://doi.org/10.1016/j.biopha.2018.03.091.
4. Zhang, L., Li, Y., Guan, C.-Y., Tian, S., Lv, X.-D., Li, J.-H., Ma, X., and Xia, H.-F. (2018). Therapeutic effect of human umbilical cord-derived mesenchymal stem cells on injured rat endometrium during its chronic phase. Stem Cell Res. Ther. *9*, 36. https://doi.org/10.1186/s13287-018-0777-5.
5. Su, J., Ding, L., Cheng, J., Yang, J., Li, X., Yan, G., Sun, H., Dai, J., and Hu, Y. (2016). Transplantation of adipose-derived stem cells combined with collagen scaffolds restores ovarian function in a rat model of premature ovarian insufficiency. Hum. Reprod. *31*, 1075–1086. https://doi.org/10.1093/humrep/dew041.
6. Kilic, S., Yuksel, B., Pinarli, F., Albayrak, A., Boztok, B., and Delibasi, T. (2014). Effect of stem cell application on Asherman syndrome, an experimental rat model. J. Assist. Reprod. Genet. *31*, 975–982. https://doi.org/10.1007/s10815-014-0268-2.
7. Santamaria, X., Cabanillas, S., Cervelló, I., Arbona, C., Raga, F., Ferro, J., Palmero, J., Remohí, J., Pellicer, A., and Simón, C. (2016). Autologous cell therapy with CD133+ bone marrow-derived stem cells for refractory Asherman's syndrome and endometrial atrophy: a pilot cohort study. Hum. Reprod.

*31*, 1087–1096. https://doi.org/10.1093/humrep/dew042.

8. Cervelló, I., Gil-Sanchis, C., Santamaría, X., Cabanillas, S., Díaz, A., Faus, A., Pellicer, A., and Simón, C. (2015). Human CD133+ bone marrow-derived stem cells promote endometrial proliferation in a murine model of Asherman syndrome. Fertil. Steril. *104*, 1552–1560.e3. https://doi.org/10.1016/j.fertnstert.2015.08.032.
9. Santamaria, X., Mas, A., Cervelló, I., Taylor, H., and Simon, C. (2018). Uterine stem cells: from basic research to advanced cell therapies. Hum. Reprod. Update *24*, 673–693. https://doi.org/10.1093/humupd/dmy028.
10. Jung, J.W., Kwon, M., Choi, J.C., Shin, J.W., Park, I.W., Choi, B.W., and Kim, J.Y. (2013). Familial Occurrence of Pulmonary Embolism after Intravenous, Adipose Tissue-Derived Stem Cell Therapy. Yonsei Med. J. *54*, 1293–1296. https://doi.org/10.3349/ymj.2013.54.5.1293.
11. Xin, L., Zheng, X., Chen, J., Hu, S., Luo, Y., Ge, Q., Jin, X., Ma, L., and Zhang, S. (2022). An Acellular Scaffold Facilitates Endometrial Regeneration and Fertility Restoration via Recruiting Endogenous Mesenchymal Stem Cells. Adv. Healthcare Mater. *11*, 2201680. https://doi.org/10.1002/adhm.202201680.
12. Cen, J., Zhang, Y., Bai, Y., Ma, S., Zhang, C., Jin, L., Duan, S., Du, Y., and Guo, Y. (2022). Research progress of stem cell therapy for endometrial injury. Mater. Today. Bio *16*, 100389. https://doi.org/10.1016/j.mtbio.2022.100389.
13. Gil-Sanchis, C., Cervelló, I., Khurana, S., Faus, A., Verfaillie, C., and Simón, C. (2015). Contribution of different bone marrow-derived cell types in endometrial regeneration using an irradiated murine model. Fertil. Steril. *103*, 1596–1605.e1. https://doi.org/10.1016/j.fertnstert.2015.02.030.
14. Gharibeh, N., Aghebati-Maleki, L., Madani, J., Pourakbari, R., Yousefi, M., and Ahmadian Heris, J. (2022). Cell-based therapy in thin endometrium and Asherman syndrome. Stem Cell Res. Ther. *13*, 33. https://doi.org/10.1186/s13287-021-02698-8.
15. Esfandyari, S., Chugh, R.M., Park, H.S., Hobeika, E., Ulin, M., and Al-Hendy, A. (2020). Mesenchymal Stem Cells as a Bio Organ for Treatment of Female Infertility. Cells *9*, 2253. https://doi.org/10.3390/cells9102253.
16. Sun, B., Ma, Y., Wang, F., Hu, L., and Sun, Y. (2019). miR-644-5p carried by bone mesenchymal stem cell-derived exosomes targets regulation of p53 to inhibit ovarian granulosa cell apoptosis. Stem Cell Res. Ther. *10*, 360. https://doi.org/10.1186/s13287-019-1442-3.
17. Chen, J.M., Huang, Q.Y., Zhao, Y.X., Chen, W.H., Lin, S., and Shi, Q.Y. (2021). The Latest Developments in Immunomodulation of Mesenchymal Stem Cells in the Treatment of Intrauterine Adhesions, Both Allogeneic and Autologous. Front. Immunol. *12*, 785717. https://doi.org/10.3389/fimmu.2021.785717.
18. Shao, X., Taha, I.N., Clauser, K.R., Gao, Y.T., and Naba, A. (2020). MatrisomeDB: the ECM-protein knowledge database. Nucleic Acids Res. *48*, D1136–D1144. https://doi.org/10.1093/nar/gkz849.
19. McCabe, M.C., Saviola, A.J., and Hansen, K.C. (2022). A mass spectrometry-based atlas of extracellular matrix proteins across 25 mouse organs. Mol. Biol. *22*, 790–801. https://doi.org/10.1101/2022.03.04.482898.
20. Jiang, Y., Zhang, H., Wang, J., Liu, Y., Luo, T., and Hua, H. (2022). Targeting extracellular matrix stiffness and mechanotransducers to improve cancer therapy. J. Hematol. Oncol. *15*, 34. https://doi.org/10.1186/s13045-022-01252-0.
21. Sanderson, P.A., Critchley, H.O.D., Williams, A.R.W., Arends, M.J., and Saunders, P.T.K. (2017). New concepts for an old problem: the diagnosis of endometrial hyperplasia. Hum. Reprod. Update *23*, 232–254. https://doi.org/10.1093/humupd/dmw042.
22. Islam, M.S., Ciavattini, A., Petraglia, F., Castellucci, M., and Ciarmela, P. (2018). Extracellular matrix in uterine leiomyoma pathogenesis: a potential target for future therapeutics. Hum. Reprod. Update *24*, 59–85. https://doi.org/10.1093/humupd/dmx032.
23. Lin, C., Tao, B., Deng, Y., He, Y., Shen, X., Wang, R., Lu, L., Peng, Z., Xia, Z., and Cai, K. (2019). Matrix promote mesenchymal stromal cell migration with improved deformation via nuclear stiffness decrease. Biomaterials *217*, 119300. https://doi.org/10.1016/j.biomaterials.2019.119300.
24. Blondel, D., and Lutolf, M.P. (2019). Bioinspired Hydrogels for 3D Organoid Culture. Chimia *73*, 81–85. https://doi.org/10.2533/chimia.2019.81.
25. Wang, J., Yang, C., Xie, Y., Chen, X., Jiang, T., Tian, J., Hu, S., and Lu, Y. (2021). Application of Bioactive Hydrogels for Functional Treatment of Intrauterine Adhesion. Front. Bioeng. Biotechnol. *9*, 760943. https://doi.org/10.3389/fbioe.2021.760943.
26. Mansour, A., Darwiche, W., Yaker, L., Da Nascimento, S., Gomila, C., Rossi, C., Jung, V., Sonnet, P., Kamel, S., Guerrera, I.C., et al. (2020). GFOGER Peptide Modifies the Protein Content of Extracellular Vesicles and Inhibits Vascular Calcification. Front. Cell Dev. Biol. *8*, 589761. https://doi.org/10.3389/fcell.2020.589761.
27. Lutolf, M.P., Lauer-Fields, J.L., Schmoekel, H.G., Metters, A.T., Weber, F.E., Fields, G.B., and Hubbell, J.A. (2003). Synthetic matrix metalloproteinase-sensitive hydrogels for the conduction of tissue regeneration: Engineering cell-invasion characteristics. Proc. Natl. Acad. Sci. USA *100*, 5413–5418. https://doi.org/10.1073/pnas.0737381100.
28. Hattori, A., Hozumi, K., Ko, J.-A., Chikama, T.i., Oomikawa, K., Kato, J., Ishida, K., Hoshi, N., Katagiri, F., Kikkawa, Y., et al. (2009). Sequence specificity of the PHSRN peptide from fibronectin on corneal epithelial migration. Biochem. Biophys. Res. Commun. *379*, 346–350. https://doi.org/10.1016/j.bbrc.2008.12.057.
29. Feng, Y., and Mrksich, M. (2004). The Synergy Peptide PHSRN and the Adhesion Peptide RGD Mediate Cell Adhesion through a Common Mechanism. Biochemistry *43*, 15811–15821. https://doi.org/10.1021/bi049174+.
30. García, J.R., Quirós, M., Han, W.M., O'Leary, M.N., Cox, G.N., Nusrat, A., and García, A.J. (2019). IFN-γ-tethered hydrogels enhance mesenchymal stem cell-based immunomodulation and promote tissue repair. Biomaterials *220*, 119403. https://doi.org/10.1016/j.biomaterials.2019.119403.
31. Im, S.H., Kim, C.Y., Jung, Y., Jang, Y., and Kim, S.H. (2017). Biodegradable vascular stents with high tensile and compressive strength: a novel strategy for applying monofilaments via solid-state drawing and shaped-annealing processes. Biomater. Sci. *5*, 422–431. https://doi.org/10.1039/C7BM00011A.
32. Xiao, M., Qiu, J., Kuang, R., Zhang, B., Wang, W., and Yu, Q. (2019). Synergistic effects of stromal cell-derived factor-1α and bone morphogenetic protein-2 treatment on odontogenic differentiation of human stem cells from apical papilla cultured in the VitroGel 3D system. Cell Tissue Res. *378*, 207–220. https://doi.org/10.1007/s00441-019-03045-3.
33. Rafael, D., Andrade, F., Martinez-Trucharte, F., Basas, J., Seras-Franzoso, J., Palau, M., Gomis, X., Pérez-Burgos, M., Blanco, A., López-Fernández, A., et al. (2019). Sterilization Procedure for Temperature-Sensitive Hydrogels Loaded with Silver Nanoparticles for Clinical Applications. Nanomaterials *9*, 380. https://doi.org/10.3390/nano9030380.
34. Cao, Y., Sun, H., Zhu, H., Zhu, X., Tang, X., Yan, G., Wang, J., Bai, D., Wang, J., Wang, L., et al. (2018). Allogeneic cell therapy using umbilical cord MSCs on collagen scaffolds for patients with recurrent uterine adhesion: a phase I clinical trial. Stem Cell Res. Ther. *9*, 192. https://doi.org/10.1186/s13287-018-0904-3.
35. Lin, Y., Li, Y., Chen, P., Zhang, Y., Sun, J., Sun, X., Li, J., Jin, J., Xue, J., Zheng, J., et al. (2023). Exosome-Based Regimen Rescues Endometrial Fibrosis in Intrauterine Adhesions Via Targeting Clinical Fibrosis Biomarkers. Stem Cells Transl. Med. *12*, 154–168. https://doi.org/10.1093/stcltm/szad007.
36. Wang, L., Yu, C., Chang, T., Zhang, M., Song, S., Xiong, C., Su, P., and Xiang, W. (2020). In situ repair abilities of human umbilical cord–derived mesenchymal stem cells and autocrosslinked hyaluronic acid gel complex in rhesus monkeys with intrauterine adhesion. Sci. Adv. *6*, eaba6357. https://doi.org/10.1126/sciadv.aba6357.
37. Xu, L., Ding, L., Wang, L., Cao, Y., Zhu, H., Lu, J., Li, X., Song, T., Hu, Y., and Dai, J. (2017). Umbilical cord-derived mesenchymal stem cells on scaffolds facilitate collagen degradation via upregulation of MMP-9 in rat uterine scars. Stem Cell Res. Ther. *8*, 84. https://doi.org/10.1186/s13287-017-0535-0.
38. Xia, H., Li, X., Gao, W., Fu, X., Fang, R.H., Zhang, L., and Zhang, K. (2018). Tissue repair and regeneration with endogenous stem cells. Nat. Rev. Mater. *3*, 174–193. https://doi.org/10.1038/s41578-018-0027-6.
39. Sha, Y., Haensel, D., Gutierrez, G., Du, H., Dai, X., and Nie, Q. (2019). Intermediate cell states in epithelial-to-mesenchymal transition. Phys. Biol. *16*, 021001. https://doi.org/10.1088/1478-3975/aaf928.
40. Zhou, Z., Wang, H., Zhang, X., Song, M., Yao, S., Jiang, P., Liu, D., Wang, Z., Lv, H., Li, R., et al. (2022). Defective autophagy contributes to endometrial epithelial-mesenchymal transition in intrauterine adhesions. Autophagy *18*, 2427–2442. https://doi.org/10.1080/15548627.2022.2038994.
41. Xu, J., Lamouille, S., and Derynck, R. (2009). TGF-β-induced epithelial to mesenchymal transition. Cell Res. *19*, 156–172. https://doi.org/10.1038/cr.2009.5.
42. Fatehullah, A., Terakado, Y., Sagiraju, S., Tan, T.L., Sheng, T., Tan, S.H., Murakami, K., Swathi, Y., Ang, N., Rajarethinam, R., et al. (2021). A tumour-resident Lgr5+ stem-cell-like pool drives the establishment and progression of advanced gastric cancers.

Nat. Cell Biol. *23*, 1299–1313. https://doi.org/10.1038/s41556-021-00793-9.
43. Tian, X., Wang, J., Jiang, L., Jiang, Y., Xu, J., and Feng, X. (2022). Chemokine/GPCR Signaling-Mediated EMT in Cancer Metastasis. JAMA Oncol. *2022*, 2208176. https://doi.org/10.1155/2022/2208176.
44. Cook, D.P., and Vanderhyden, B.C. (2020). Context specificity of the EMT transcriptional response. Nat. Commun. *11*, 2142. https://doi.org/10.1038/s41467-020-16066-2.
45. Chakraborty, P., George, J.T., Tripathi, S., Levine, H., and Jolly, M.K. (2020). Comparative Study of Transcriptomics-Based Scoring Metrics for the Epithelial-Hybrid-Mesenchymal Spectrum. Front. Bioeng. Biotechnol. *8*, 220. https://doi.org/10.3389/fbioe.2020.00220.
46. López-Novoa, J.M., and Nieto, M.A. (2009). Inflammation and EMT: an alliance towards organ fibrosis and cancer progression. EMBO Mol. Med. *1*, 303–314. https://doi.org/10.1002/emmm.200900043.
47. de Miguel-Gómez, L., López-Martínez, S., Francés-Herrero, E., Rodríguez-Eguren, A., Pellicer, A., and Cervelló, I. (2021). Stem Cells and the Endometrium: From the Discovery of Adult Stem Cells to Pre-Clinical Models. Cells *10*, 595. https://doi.org/10.3390/cells10030595.
48. Masuda, H., Anwar, S.S., Bühring, H.-J., Rao, J.R., and Gargett, C.E. (2012). A Novel Marker of Human Endometrial Mesenchymal Stem-Like Cells. Cell Transplant. *21*, 2201–2214. https://doi.org/10.3727/096368911X637362.
49. Tempest, N., Maclean, A., and Hapangama, D.K. (2018). Endometrial Stem Cell Markers: Current Concepts and Unresolved Questions. Int. J. Mol. Sci. *19*, 3240. https://doi.org/10.3390/ijms19103240.
50. Huch, M., Dorrell, C., Boj, S.F., van Es, J.H., Li, V.S.W., van de Wetering, M., Sato, T., Hamer, K., Sasaki, N., Finegold, M.J., et al. (2013). In vitro expansion of single Lgr5+ liver stem cells induced by Wnt-driven regeneration. Nature *494*, 247–250. https://doi.org/10.1038/nature11826.
51. Fitzgerald, H.C., Dhakal, P., Behura, S.K., Schust, D.J., and Spencer, T.E. (2019). Self-renewing endometrial epithelial organoids of the human uterus. Proc. Natl. Acad. Sci. USA *116*, 23132–23142. https://doi.org/10.1073/pnas.1915389116.
52. Wang, W., Vilella, F., Alama, P., Moreno, I., Mignardi, M., Isakova, A., Pan, W., Simon, C., and Quake, S.R. (2020). Single-cell transcriptomic atlas of the human endometrium during the menstrual cycle. Nat. Med. *26*, 1644–1653. https://doi.org/10.1038/s41591-020-1040-z.
53. Fonseca, M.A.S., Haro, M., Wright, K.N., Lin, X., Abbasi, F., Sun, J., Hernandez, L., Orr, N.L., Hong, J., Choi-Kuaea, Y., et al. (2023). Single-cell transcriptomic analysis of endometriosis. Nat. Genet. *55*, 255–267. https://doi.org/10.1038/s41588-022-01254-1.
54. Tan, Y., Flynn, W.F., Sivajothi, S., Luo, D., Bozal, S.B., Davé, M., Luciano, A.A., Robson, P., Luciano, D.E., and Courtois, E.T. (2022). Single-cell analysis of endometriosis reveals a coordinated transcriptional programme driving immunotolerance and angiogenesis across eutopic and ectopic tissues. Nat. Cell Biol. *24*, 1306–1318. https://doi.org/10.1038/s41556-022-00961-5.
55. Cao, D.-D., Wang, J., Yao, Y.-Q., and Yeung, W.S.-B. (2022). Single-cell analysis in endometrial research. Reprod. Dev. Med. *6*, 197–207. https://doi.org/10.1097/RD9.0000000000000037.
56. Cochrane, D.R., Campbell, K.R., Greening, K., Ho, G.C., Hopkins, J., Bui, M., Douglas, J.M., Sharlandjieva, V., Munzur, A.D., Lai, D., et al. (2020). Single cell transcriptomes of normal endometrial derived organoids uncover novel cell type markers and cryptic differentiation of primary tumours. J. Pathol. *252*, 201–214. https://doi.org/10.1002/path.5511.
57. Mucenski, M.L., Mahoney, R., Adam, M., Potter, A.S., and Potter, S.S. (2019). Single cell RNA-seq study of wild type and Hox9,10,11 mutant developing uterus. Sci. Rep. *9*, 4557. https://doi.org/10.1038/s41598-019-40923-w.
58. Lv, H., Zhao, G., Jiang, P., Wang, H., Wang, Z., Yao, S., Zhou, Z., Wang, L., Liu, D., Deng, W., et al. (2022). Deciphering the endometrial niche of human thin endometrium at single-cell resolution. Proc. Natl. Acad. Sci. USA *119*, e2115912119. https://doi.org/10.1073/pnas.2115912119.
59. Santamaria, X., Roson, B., Perez-Moraga, R., Venkatesan, N., Pardo-Figuerez, M., Gonzalez-Fernandez, J., Llera-Oyola, J., Fernández, E., Moreno, I., Salumets, A., et al. (2023). Decoding the endometrial niche of Asherman's Syndrome at single-cell resolution. Nat. Commun. *14*, 5890. https://doi.org/10.1038/s41467-023-41656-1.
60. Garcia-Alonso, L., Handfield, L.-F., Roberts, K., Nikolakopoulou, K., Fernando, R.C., Gardner, L., Woodhams, B., Arutyunyan, A., Polanski, K., Hoo, R., et al. (2021). Mapping the temporal and spatial dynamics of the human endometrium in vivo and in vitro. Nat. Genet. *53*, 1698–1711. https://doi.org/10.1038/s41588-021-00972-2.
61. Flum, M., Dicks, S., Teng, Y.-H., Schrempp, M., Nyström, A., Boerries, M., and Hecht, A. (2022). Canonical TGFβ signaling induces collective invasion in colorectal carcinogenesis through a Snail1- and Zeb1-independent partial EMT. Oncogene *41*, 1492–1506. https://doi.org/10.1038/s41388-022-02190-4.
62. Cao, J., Liu, D., Zhao, S., Yuan, L., Huang, Y., Ma, J., Yang, Z., Shi, B., Wang, L., and Wei, J. (2020). Estrogen attenuates TGF-β1-induced EMT in intrauterine adhesion by activating Wnt/β-catenin signaling pathway. Braz. J. Med. Biol. Res. *53*, e9794. https://doi.org/10.1590/1414-431x20209794.
63. Lee, W.-L., Liu, C.-H., Cheng, M., Chang, W.-H., Liu, W.-M., and Wang, P.-H. (2021). Focus on the Primary Prevention of Intrauterine Adhesions: Current Concept and Vision. Indian J. Manag. Sci. *22*, 5175. https://doi.org/10.3390/ijms22105175.
64. Cindrova-Davies, T., Zhao, X., Elder, K., Jones, C.J.P., Moffett, A., Burton, G.J., and Turco, M.Y. (2021). Menstrual flow as a non-invasive source of endometrial organoids. Commun. Biol. *4*, 651–658. https://doi.org/10.1038/s42003-021-02194-y.
65. Mukhopadhyay, C., Zhao, X., Maroni, D., Band, V., and Naramura, M. (2013). Distinct Effects of EGFR Ligands on Human Mammary Epithelial Cell Differentiation. PLoS One *8*, e75907. https://doi.org/10.1371/journal.pone.0075907.
66. Wee, P., and Wang, Z. (2017). Epidermal Growth Factor Receptor Cell Proliferation Signaling Pathways. Cancers *9*, 52. https://doi.org/10.3390/cancers9050052.
67. Schramm, F., Schaefer, L., and Wygrecka, M. (2022). EGFR Signaling in Lung Fibrosis. Cells *11*, 986. https://doi.org/10.3390/cells11060986.
68. Traverse, S., Gomez, N., Paterson, H., Marshall, C., and Cohen, P. (1992). Sustained activation of the mitogen-activated protein (MAP) kinase cascade may be required for differentiation of PC12 cells. Comparison of the effects of nerve growth factor and epidermal growth factor. Biochem. J. *288*, 351–355.
69. Barberán, S., and Cebrià, F. (2019). The role of the EGFR signaling pathway in stem cell differentiation during planarian regeneration and homeostasis. Semin. Cell Dev. Biol. *87*, 45–57. https://doi.org/10.1016/j.semcdb.2018.05.011.
70. Moustakas, A., and Heldin, C.-H. (2016). Mechanisms of TGFβ-Induced Epithelial–Mesenchymal Transition. J. Clin. Med. *5*, 63. https://doi.org/10.3390/jcm5070063.
71. Singh, P., Metkari, S., and Bhartiya, D. (2022). Additional evidence to support OCT-4 positive VSELs and EnSCs as the elusive tissue-resident stem/progenitor cells in adult mice uterus. Stem Cell Res. Ther. *13*, 60. https://doi.org/10.1186/s13287-022-02703-8.
72. Bhartiya, D., Singh, P., Sharma, D., and Kaushik, A. (2022). Very small embryonic-like stem cells (VSELs) regenerate whereas mesenchymal stromal cells (MSCs) rejuvenate diseased reproductive tissues. Stem Cell Rev. Rep. *18*, 1718–1727. https://doi.org/10.1007/s12015-021-10243-6.

## STAR★METHODS

### KEY RESOURCES TABLE

| REAGENT or RESOURCE | SOURCE | IDENTIFIER |
|---|---|---|
| Antibodies | | |
| E-cadherin | CST | Cat# 3195; RRID: AB_2291471 |
| E-cadherin | Abcam | Cat# ab231303; RRID: AB_2923285 |
| Pan-Keratin | CST | Cat# 4545; RRID: AB_490860 |
| Vimentin | Abcam | Cat# ab92547; RRID:AB_10562134 |
| LGR5 | Origene | Cat# TA503316S; RRID:AB_2723318 |
| Estrogen Receptor α (ERα) | Abcam | Cat# ab108398; RRID:AB_2728817 |
| N-cadherin | CST | Cat# 13116; RRID:AB_2687616 |
| N-cadherin | Proteintech | Cat# 66219-1 |
| LAMA3 | Abcam | Cat# ab151715 |
| Ki67 | Abcam | Cat# ab16667; RRID:AB_302459 |
| Ki67 | Abcam | Cat# ab279653; RRID:AB_2934265 |
| RPS4Y1 | Proteintech | Cat# 17296-1-AP |
| MAPK (Erk1/2) | CST | Cat# 4370; RRID:AB_2315112 |
| PE anti-human CD133 | BioLegend | Cat# 393903; AB_2734477 |
| PE anti-human LGR5 | BioLegend | Cat# 373803; AB_2686987 |
| PE anti-human CD324 (E-cadherin) | BioLegend | Cat# 324105; AB_756067 |
| Chemicals, peptides, and recombinant proteins | | |
| Penicillin/Streptomycin | Gibco | Cat# 15070063 |
| Y-27632 | AbMole BioScience | Cat# 129830-38-2 |
| A83-01 | AbMole BioScience | Cat# M5037 |
| SB202190 | AbMole BioScience | Cat# M2062 |
| Nicotinamide | Sigma-Aldrich | Cat# N0636-100G |
| Recombinant human EGF | PeproTech | Cat# 100-47 |
| Recombinant human Noggin | PeproTech | Cat# 120-10C |
| Recombinant human FGF-10 | PeproTech | Cat# 100-26 |
| Recombinant human R-Spondin-1 | PeproTech | Cat# 120-38 |
| Recombinant Wnt-3a | PeproTech | Cat# 315-20 |
| Recombinant Wnt-7a | PeproTech | Cat# 120-31 |
| Recombinant TGF-α | PeproTech | Cat# 100-16A |
| N-acetyl-L-cysteine | Sigma-Aldrich | Cat# A9165 |
| Recombinant Human TGF-β1 | PeproTech | Cat# 100-21 |
| Recombinant Human TNF-α | PeproTech | Cat# 300-01A |
| Critical commercial assays | | |
| Advanced DMEM/F-12 | Gibco | Cat# 12634010 |
| N-2 supplement | Gibco | Cat# 17502048 |
| B-27 supplement minus vitamin A | Gibco | Cat# 17504044 |
| ITS Liquid Media Supplement | Sigma-Aldrich | Cat# I3146 |
| Serum-free Medium for MSCs | Baso Biotech | Cat# 04304P05 |
| Advanced cell culture supplement | AventaCell | Cat# HPCFDCRL50 |
| GlutaMAX | Gibco | Cat# 35050061 |

(*Continued on next page*)

*Continued*

| REAGENT or RESOURCE | SOURCE | IDENTIFIER |
|---|---|---|
| Rat TIMP-1 ELISA Kit | Ray Biotech | Cat# ELR-TIMP1-1 |
| Rat CTGF ELISA Kit | Abcam | Cat# ab275897 |
| Human TGFA ELISA Kit | Weiao Biotech | Cat# EH10461 |
| Human Wnt7A ELISA Kit | Weiao Biotech | Cat# EH11211 |
| RIPA lysis buffer | Weiao Biotech | Cat# WB0101 |
| Proteases inhibitor cocktail | Weiao Biotech | Cat# WB0122 |
| BCA Protein Assay kit | Weiao Biotech | Cat# WB0123 |
| CFSE Cell Division Tracker Kit | BioLegend | Cat# 423801 |
| Cell Recovery Solution | Corning | 354253 |
| Cell Counting Kit-8 | Servicebio | G4103-1ML |
| Luminescent Cell Viability Assay | Promega | G9241 |
| Experimental models: Cell lines | | |
| Rat: Sprague-Dawley | SLAC Animal | Slac:SD |
| UC-MSC | SNC Stemcell Biotech | ELPIS UC-MSC Injection |
| Software and algorithms | | |
| GraphPad Prism | GraphPad Prism 8.0 | https://www.graphpad.com |
| R | R 4.2.2 | https://www.r-project.org |
| ImageJ | ImageJ with Java 8 | https://imagej.nih.gov/ij/ |
| Image-Pro Plus | Image-Pro Plus 6.0.0.260 | https://mediacy.com/image-pro/ |
| FCS Express | FCS Express 7 | https://denovosoftware.com/ |
| Adobe Illustrator | Adobe Illustrator 2017 | https://www.adobe.com/ |

## RESOURCE AVAILABILITY

### Lead contact

Further information and requests for resources should be directed to and will be fulfilled by the lead contact, Li Liu (liulisipi@foxmail.com).

### Materials availability

This study did not generate new unique reagents.

### Data and code availability

- All data reported in this paper will be shared by the lead contact upon request.
- This paper does not report original code.
- Any additional information required to reanalyze the data reported in this paper is available from the lead contact upon request.

## EXPERIMENTAL MODEL AND STUDY PARTICIPANT DETAILS

### Establishment and treatment of uterine injury rat model

All animal experiments were approved by Animal Experimental Ethical Inspection of SIPI. 50 female Sprague-Dawley rats (8 weeks old) were used in this experiment, which was divided into five groups: uterine injury model group (Uterine Injury), hydrogel control group (Hydrogel), UCMSC+ hydrogel treatment group (UCMSC+ hydrogel), UCMSC solution direct injection group (UCMSC) and blank control group (Blank). During the estrous phase of SD rats, 40 rats were anesthetized, and then incisions were made along the midline of the abdomen of rats to expose the uterus. The tip of the 1mL syringe was partially bent in advance and then inserted into the 1/3 of the distance from the connection between the left and right uterus. Back and forth rotational scraping was performed 8 times, and the depth of scraping was about 2/3 of the uterine wall until bleeding was visible to the naked eye in both the left and right uterus (Roughness appears when scraping at this point). The abdominal cavity was washed with 0.9% (w/v) normal saline after the surgery, and the abdomen was sutured. After 7 days, the uterus was re-exposed to confirm the formation of intrauterine adhesions and then enrolled into the group of uterine injury, hydrogel, UCMSC+ hydrogel and UCMSC (10 rats in each group). Subsequently, 1mL normal saline (uterine injury group), hydrogel without UC-MSCs (Hydrogel group), hydrogel loaded $5\times10^6$ UC-MSCs (UCMSC+ hydrogel group) and UC-MSCs solution (UCMSC group) were added to the adhesion sites of the uterus.

## METHOD DETAILS

### Proteomic analysis

#### *Sample preparation*

The uterine tissue were excised from 4 healthy SD rats during the estrous interphase. Tissues were then weighed, minced and resuspended in ice-cold RIPA lysis buffer (Weiao Biotech) supplemented with proteases inhibitor cocktail (Weiao Biotech). Subsequently, transfer the buffer to a shaker, followed by ice incubation for 1 hour, then subject it to centrifugation at 12,000 g for 10 minutes to collect the supernatant. The protein concentration was determined using a BCA Protein Assay Kit (Weiao Biotech). Proteins were reduced in 5 mM dithiothreitol at 56°C for 30 min and then alkylated in 15 mM iodoacetamide at room temperature for 30 min in darkness. Reaction was quenched with 30 mM cysteine at room temperature for additional 30 min. Protein samples underwent trypsin digestion (enzyme-to-substrate ratio of 1:50 at 37°C for 16 hours) followed by desalting through MonoSpin C18 cartridges and vacuum-dried by Speed Vac. The peptide residues were reconstituted in water containing 0.1% formic acid and were centrifuged at 14,000 rpm for 10 min prior to Nano-LC-MS/MS analysis.

#### *LC-MS/MS*

Peptide samples were analyzed on a nano-LC system (Bruker Daltonics) with C18 nano-capillary analytical column (250 mm × 75 μm) (IonOptiks) heated at 50°C in a column oven. Mobile phases consisted of 0.1% (v/v) formic acid in water (phase A) and in acetonitrile (phase B). Samples were separated by a 60 min stepped gradient ranging from 2 to 30% B at a flow rate of 400 nL/min. Peptides were detected on a timsTOF Pro instrument (Bruker Daltonics) operated in PASEF mode. TIMS accumulation time and ion mobility separation time were both set at a fixed value of 100 ms. The range of mobility values was 0.45–1.45 vs./cm2 (1/K0), and the covered m/z range was 100–1700 m/z. Subsequently, MS raw files were searched against the UniProt Rattus norvegicus proteome database using PaSER (version 1.0) software. The protease was trypsin, with a maximum allowance of 2 missed cleavages. Carbamidomethyl (C) was considered as a fixed modification, while oxidation (M) and acetylation (protein N-term) were treated as variable modifications. Employing the target-decoy strategy, the thresholds of false discovery rate (FDR) for proteins and peptides were 0.01. Finally, the matrisome proteins were filtered according to the ECM matrisome database.

### Synthesis of ECM-adhesion mimic hydrogel and encapsulation of UC-MSC in hydrogels

8-arm PEG Maleimide (20 kDa) and SH-PEG-SH (2 kDa) were purchased from Adamas life. Peptides were synthesized and purified by QYAOBIO and CSBio. These peptides were used in the hydrogel: SH-GPC$(GPP)_5$GE-(Hyp)-GFR$(GPP)_5$GPC (GFOGER); SH-PHSRN (PHSRN); SH-YIGSR (YIGSR); SH-GRGDS (GRGDS).

#### *Synthesis of ECM-adhesion mimic hydrogel*

GFOGER peptide (2 mM), YIGSR peptide (2 mM), PHSRN peptide (2 mM), GRGDS peptide (3 mM) and cross-linker SH-PEG-SH (2 kDa, 5 mM, 5%) were dissolved in the MSC medium. Subsequently, 8-arm PEG Maleimide (20 kDa, 5 mM) were added to the solution, followed by incubation for 15 min to synthesize hydrogel.

#### *Encapsulation of UC-MSCs in hydrogels*

UC-MSCs were resuspended in peptide solution. Subsequently, 8-arm PEG Maleimide were added to the solution, followed by incubation for 15 min to encapsulate MSCs within the hydrogel.

### Culture and establishment of EEOs and EMT induced EEOs

#### *EEOs culture from human endometrium*

The study was approved by the Medical Research Ethics Committee of International Peace Maternal and Child Health Hospital. All participants provided written informed consent for sample collection. Patients taking any hormones were excluded from the study. 2 patients of 48–49 years of age diagnosed with endometrial cancer were enrolled. Normal endometrium tissues (all with normal menstrual cycle) from proliferative phases were collected from the normal part of uterus (Table S1). The endometrial tissues of 1-2 cm in length, 1-2 cm in width and 1-2 cm in depth were cut and transported to the laboratory at a temperature of 4°C. Tissues were then carefully minced into small cubes. Subsequently, tissues were added to 10 mL of Advanced DMEM/F12 (Gibco) medium supplemented with Dispase (1.25 U/mL; Stemcell) and Collagenase IV (2.5 mg/mL; Sigma), followed by gentle shaking at 37°C for 1 hour. To quench the digestion process, an equal volume of DMEM medium containing 10% FBS (Gibco) was added. After complete dissociation, the undigested tissues were allowed to settle for 5 minutes to remove. Endometrial glands/epithelial cells and stromal cells were isolated by filter-separated. The supernatant was passed through 100 μm cell strainers. Wash through well with Advanced DMEM/F12. Then invert the strainers over a petri dish and backwash the glandular/epithelial cells. Transfer the backwashed glands/epithelial cells to a universal tube, followed by centrifugation at 300g for 5 min. After centrifugation and subsequent washing with PBS, the pellet was resuspended in EEO medium with 70% Matrigel at a density of 10,000 cells per 100 μL. The culture medium was changed every 3 days using EEO medium composed of DMEM/F12 (Gibco), penicillin/streptomycin (100 U/L; Gibco), HEPES (10 mM; Gibco), GlutaMAX (1×; Gibco) , B27 supplement (1×; Gibco), N2 supplement (1×; Gibco), ITS Liquid Media Supplement (1×; Sigma–Aldrich), Nicotinamide (1 mM; Sigma–Aldrich), N-acetylcysteine-1 (1.25 mM; Sigma–Aldrich), EGF (50 ng/mL;

Peprotech), FGF-10 (100 ng/mL; Peprotech), Wnt3a (200 ng/mL; Peprotech), Noggin (100 ng/mL; Peprotech), Rspondin-1 (200 ng/mL; Peprotech), Y-27632 (9 μM; AbMole BioScience), A83-01 (500 nM; AbMole BioScience), SB202190 (10 μM; AbMole BioScience). Following a 14-day culture period, EEOs could be released from Matrigel using Dispase (1U/mL; Stemcell) for 1 hour at 37°C. Subsequently, Tryple (Gibco) was used to further dissociated the organoids into single cells within 10 minutes before passaging them at a ratio of 1:3.

### *Establishment of EMT induced EEOs model*

Before induction, EEOs were released from Matrigel using Dispase (1 U/mL; Stemcell) for 1 hour at 37°C. Released EEOs were incubated with Tryple (Gibco) and Trypsin (0.25%; Gibco) for 5 min at 37 °C. After centrifugation (300g, 5 min) without quenching the incubation, the EEOs were resuspended in EMT medium with 50% Matrigel. The EMT medium contained DMEM/F12 (Gibco), penicillin/streptomycin (100 U/L; Gibco), HEPES (10 mM; Gibco), GlutaMAX (1×; Gibco) , B27 supplement (1×; Gibco), N2 supplement (1×; Gibco), ITS Liquid Media Supplement (1×; Sigma–Aldrich), Nicotinamide (1 mM; Sigma–Aldrich), N-acetylcysteine-1 (1.25 mM; Sigma–Aldrich), TGF-β1 (100 ng/mL; Peprotech), TNF-α (100 ng/mL; Peprotech). After a 96-hour induction period, the EEOs were utilized for subsequent experiments and validation of mesenchymal markers.

## Co-culture experiment of EEO and UC-MSCs

### *Co-culture of normal EEOs and UC-MSCs*

EEOs were released from Matrigel using Dispase (1 U/mL; Stemcell) and subsequently resuspended in EEO medium. For co-culture assay, UC-MSCs were directly added to the EEOs solution at predetermined ratios. The number and diameter of organoids were calculated using ImageJ. For live imaging, UC-MSCs were resuspended in CFSE solution and then cells were incubated for 20 minutes at 37°C in the dark. Incubated UC-MSCs were added to the EEOs solution at predetermined ratios. Live imaging was conducted using confocal fluorescence screening via Nikon ECLIPSE Ti2. Images were obtained every 1 hour for each well till 96 hours post seeding.

### *Co-culture of EMT induced EEO and UC-MSCs*

EMT induced EEOs were released from Matrigel using Dispase (1 U/mL; Stemcell). The supernatant was passed through 40 μm cell strainers. After centrifugation and subsequent washing with PBS, EMT induced EEOs were resuspended in EMT medium. For co-culture assay, UC-MSCs were then added to the EEOs solution at 1:1 ratio. For live imaging, UC-MSCs were resuspended in CFSE solution and then cells were incubated for 20 minutes at 37°C in the dark. Incubated UC-MSCs were added to the EEOs solution at 1:1 ratio. Live imaging was conducted using confocal fluorescence screening via Nikon ECLIPSE Ti2. Images were obtained every 1 hour for each well till 96 hours post seeding.

## Immunofluorescence staining

EEOs were seeded in 24-well plates prior to immunofluorescence assay. Organoids were released from Matrigel and incubated with 1 mL of cell recovery solution at 4°C for 60 min. Organoids was resuspended and fixed in 4% PFA at room temperature for 30 min. Then, the organoids were blocked for 1 hour in the blocking solution (0.3% Triton X-100 + 0.1% Tween-20 + 5% BSA). Organoids were then incubated in 5% BSA with primary antibody per well at 4°C overnight. Then, the organoids were incubated with secondary antibody (1× concentration) diluted in 5% BSA solution for 1 h at room temperature. Finally, the organoids were incubated with DAPI for 1 h at room temperature in the dark. Organoids were washed 3 times with PBS between each of the above steps. Antibodies used for immunofluorescence staining in the study is provided in key resources table. The images were captured using a Nikon ECLIPSE Ti2. The size of the images was adjusted and assembled in Adobe Illustrator. Scale bars were indicated in the figures and legends.

The dilution information of primary antibody used was as follows: E-cadherin (CST Cat#3195) dilution: 1:500; E-cadherin (Abcam Cat# ab231303) dilution: 1:150; Pan-Keratin (CST Cat#4545) dilution: 1:150; Vimentin (Abcam Cat#ab92547)dilution: 1:100; LGR5 (Origene Cat#TA503316S) dilution: 1:100; Estrogen Receptor α (Abcam Cat#ab108398) dilution: 1:200 N-cadherin (CST Cat#13116) dilution: 1:500; N-cadherin (Proteintech Cat#66219-1) dilution: 1:50; LAMA3 (Abcam Cat#ab151715) dilution: 1:100; Ki67 (Abcam Cat#ab16667) dilution: 1:200; Ki67 (Abcam Cat#ab279653)dilution: 1:50; RPS4Y1 (Proteintech Cat# 17296-1-AP) dilution: 1:50.

## Flow cytometry analysis and cell sorting

EEOs were released from Matrigel using Dispase (1 U/mL; Stemcell) for 1 hour at 37°C. Subsequently, EEOs were resuspended in TrypLE (Gibco) and incubated at 37°C for 10 minutes to dissociate them into single cells. The cells were then suspended in PBS and sequentially incubated with blocking solution and antibody, followed by a 20-minute incubation in the dark. Analysis and cell sorting were performed using Beckman CytoFLEX and SONY MA900, and the data were analyzed with FCS Express (*De Novo* software). Antibodies used for flow cytometry in the study is provided in key resources table.

## Protein measurement by ELISA assay

Protein supernatants were collected for enzyme-linked immunosorbent assay. The ELISA kits (Raybiotech; Abcam; Weiao Biotech) for CTGF, TIMP1, Wnt7α and TGFα were used in accordance with the manufacturer's instructions.

## Western Blot

EEOs were released from Matrigel using Dispase (1 U/mL; Stemcell) for 1 hour on ice. Released EEOs were washed with ice-cold PBS for 2 times. Then, EEOs were resuspended in ice-cold RIPA lysis buffer (Weiao Biotech) supplemented with proteases inhibitor cocktail (Weiao Biotech). Subsequently, transfer the buffer to a shaker, followed by ice incubation for 1 hour, then subject it to centrifugation at 12,000 g for 10 minutes to collect the supernatant. The protein concentration was determined using a BCA Protein Assay kit (Weiao Biotech). Equivalent amounts of protein were denatured in the loading buffer through boiling, electrophoresed via SDS-PAGE gel and subsequently transferred to the PVDF membrane. The membranes were blocked with 5% BSA in TBST at room temperature for 1 hour, followed by incubation with the primary antibody overnight at 4°C and subsequent incubation with the secondary antibody at room temperature for 1 hour. Protein expression was detected using the Tanon 4600 Imaging System (Bio-Rad). Antibodies used for Western Blot in the study is provided in key resources table. The size of the images was adjusted and assembled in Adobe Illustrator.

The dilution information of primary antibody used was as follows: MAPK (Erk1/2) (CST Cat#4370) dilution: 1:2000.

## Histological analysis

Tissues and organoids were fixed in 4% PFA at room temperature for 30 min. The fixed tissues and organoids were subsequently dehydrated and embedded in paraffin wax. The paraffin-embedded tissues and organoids were sectioned at a thickness of 5 μm and subjected to hematoxylin and eosin (H&E), Masson and immunohistochemical staining.

### *H&E and Masson*

The HE and Masson staining were performed in accordance with standard protocols. Following HE staining, the number of glands and thickness of endometrium were measured at a 40× magnification. Subsequently, five fields were randomly selected at a 400× magnification and the collagen deposition ratio was measured using Image-Pro Plus.

### *Immunohistochemistry*

The paraffin sections were dewaxed and subsequently subjected to antigen retrieval by incubating in boiled citrate buffer (pH 6) for 20 minutes. Next, the sections were treated with a blocking solution at room temperature for 1 hour, followed by overnight incubation at 4°C with primary antibody. After washing, sections were incubated with secondary antibody at room temperature for 1 hour. Finally, the sections were treated with DAB solution. Then, the sections were counterstained with hematoxylin, dehydrated with an ethanol gradient, and fixed with neutral balsam. Five fields were randomly selected at a 400× magnification and the mean optical density was measured using Image-Pro Plus.

## Single-cell RNA sequencing

### *Sample preparation*

EEOs were released from Matrigel using Dispase (1 U/mL; Stemcell) for 1 hour at 37°C. Released EEOs were washed with PBS for 2 times. Then, EEOs were collected and stored in liquid nitrogen for scRNA-seq.

### *Raw scRNA-seq data processing and unsupervised clustering*

The raw scRNA-seq data were preprocessed using Cell Ranger Single Cell software suite provided by 10x Genomics, detailed QC metrics were generated and evaluated to filter cells, thereby obtaining high-quality data for subsequent analysis. Cells with low-complexity libraries (less than 500 detected genes) and cells where more than 25% of genes derived from the mitochondria were initially filtered out and excluded from further analysis. Then, doublets and multiplets were removed using DoubletFinder. Subsequently, the filtered gene cell matrix underwent library size normalization in Seurat to obtain a normalized UMI count. Seurat (LogNormalize) was applied to the normalized gene-cell matrix in order to identify highly variable genes (HVGs) for unsupervised cell clustering. Elbow plot was generated using ElbowPlot function of Seurat, and the top 20 significant principal components (PCs) were determined. Based on unsupervised clustering with Seurat's FindClusters function, we constructed the Shared Nearest Neighbor (SNN) graph using FindNeighbors function of Seurat. Subsequently, the Uniform Manifold Approximation and Projection (UMAP) method was employed along with Seurat's RunUMAP function for visualization.

### *Differential gene expression (DEG) analysis and cell type identification*

The identification of differentially expressed genes (DEGs) in each cluster was performed using FindMarkers function in Seurat. DEGs were filtered based on the following criteria: gene expression in more than 10% of cells within more abundant group, logFC (expression fold change) >0.26, and P value <0.01. To identify the cell type, we used the proved endometrial marker genes for initial identification of major cell types (epithelial cells, mesenchymal cells, and UC-MSCs). Subsequently, EMT-specific markers were utilized to further discriminate between different cell clusters. Finally, we identified organoid-specific genes by immunofluorescence.

## Cell adhension assay

UC-MSCs were resuspended in CFSE solution. Cells were incubated for 20 minutes at 37°C in the dark. For the control group, incubated cells were directly added to the 12-well plates. For the gel group, wells were precoated with hydrogel prior to cell seeding. At predetermined

time-points, the fluorescent imaging was performed using Nikon ECLIPSE Ti2. The number and area of cells were calculated using the NIS-Elements software suite.

### Cell viability assay

UC-MSCs were cultured in 96-well plates for a designated time period. For the control group, cells were directly seeded to the plates. For the gel group, cells were encapsulated within hydrogel before seeded to the plates.

For the CCK8 cell viability assay: At predetermined time-points, 10 μL CCK-8 reagent was added for 2 hours, and then the absorbance was measured at 450 nm.

For the luminescent cell viability assay: At predetermined time-points, 100 μL CellTiter-Glo® reagent was added for 10 minutes, and then record luminescence.

### Cell invasion assay

UC-MSCs were resuspended in DMEM high glucose medium. For the control group, cell suspensions (100 μL, 5000 cells/well) were encapsulated within Matrigel before seeded to the upper chamber of the Transwell plates (8 μm; Corning, USA). For the gel group, cell suspensions (100 μL, 5000 cells/well) were encapsulated within hydrogel before seeded to the upper chamber. Subsequently, 600 μL of corresponding medium supplemented with 10% FBS was added to the lower chamber. Following incubation at 37°C for a designated time period, cells in the upper chamber were carefully removed. Migrated cells were fixed with 4% PFA, stained with 0.1% crystal violet, and quantified using Image J at a 40× magnification.

## QUANTIFICATION AND STATISTICAL ANALYSIS

All data were analysed using GraphPad Prism 8.0 and presented as mean ± standard deviation (SD) of at least 3 independent experiments. Significant differences were evaluated by Student's unpaired t-test or the chisquare test for two groups. For multiple groups, significant differences were analyzed by one-way ANOVA. Statistical significance was determined at $P<0.05$ (labelled with *).